Positive Low Cloud Feedback Primarily Caused by Increasing Longwave Radiation from the Sea Surface in Two Versions of a Climate Model

Tomoo Ogura[1], Mark J Webb[2], and Adrian Lock[3]

[1]National Institute for Environmental Studies
[2]UK Met Office Hadley Centre
[3]Met Office

March 26, 2023

Abstract

Low cloud feedback in global warming projections by climate models is characterized by its positive sign, the mechanism of which is not well understood. Here we propose that the positive sign is primarily caused by the increase in upward longwave radiation from the sea surface. We devise numerical experiments that enable separation of the feedback into components coming from physically distinct causes. Results of these experiments with a climate model indicate that increases in upward longwave radiation from the sea surface cause warming and absolute drying in the boundary layer, leading to the positive low cloud feedback. The absolute drying results from decrease in surface evaporation, and also from decrease in inversion strength which enhances vertical mixing of drier free tropospheric air into the boundary layer. This mechanism is different from previously proposed understanding that positive low cloud feedback is caused by increases in surface evaporation or vertical moisture contrast.

Hosted file

959039_0_art_file_10816457_rrt1kk.docx available at https://authorea.com/users/557943/articles/630965-positive-low-cloud-feedback-primarily-caused-by-increasing-longwave-radiation-from-the-sea-surface-in-two-versions-of-a-climate-model

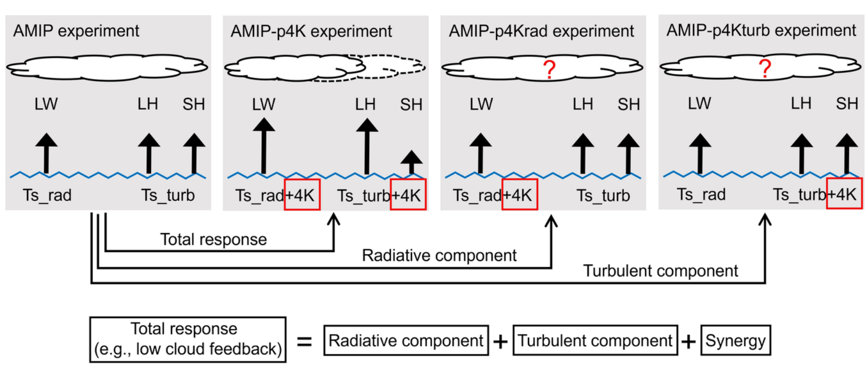

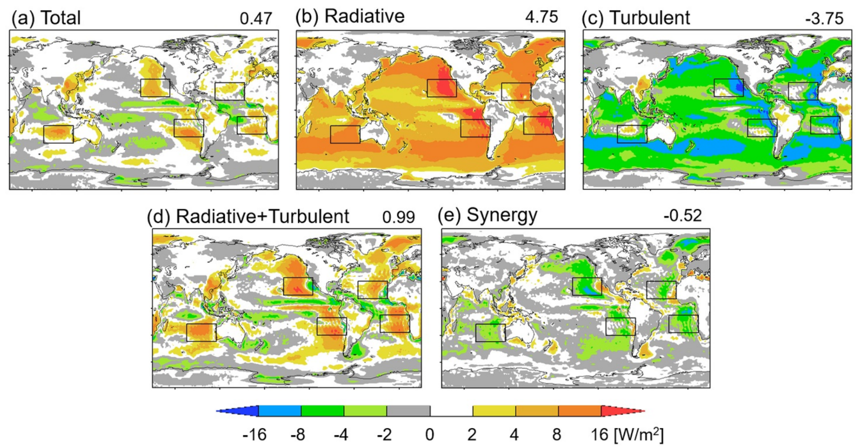
(a) Total 0.47
(b) Radiative 4.75
(c) Turbulent -3.75
(d) Radiative+Turbulent 0.99
(e) Synergy -0.52
-16 -8 -4 -2 0 2 4 8 16 [W/m²]

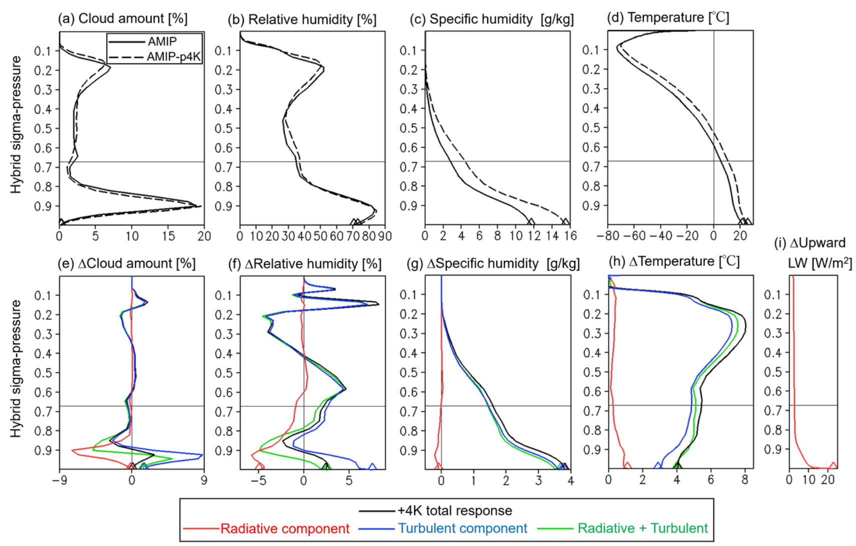
(a) Cloud amount [%]
(b) Relative humidity [%]
(c) Specific humidity [g/kg]
(d) Temperature [℃]
AMIP
AMIP-p4K
Hybrid sigma-pressure
(e) ΔCloud amount [%]
(f) ΔRelative humidity [%]
(g) ΔSpecific humidity [g/kg]
(h) ΔTemperature [℃]
(i) ΔUpward LW [W/m²]
+4K total response
Radiative component
Turbulent component
Radiative + Turbulent

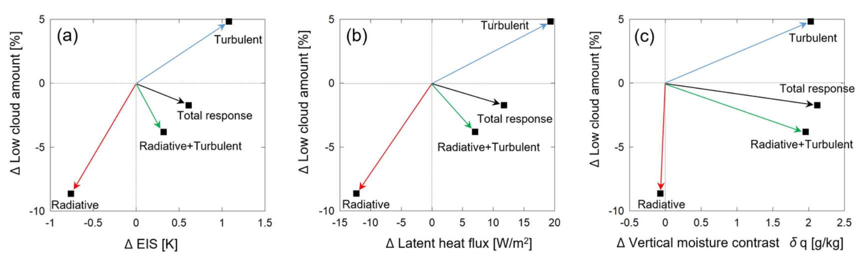
(a)
(b)
(c)
Δ Low cloud amount [%]
Turbulent
Total response
Radiative+Turbulent
Radiative
Δ EIS [K]
Δ Latent heat flux [W/m²]
Δ Vertical moisture contrast δ q [g/kg]

Positive Low Cloud Feedback Primarily Caused by Increasing Longwave Radiation from the Sea Surface in Two Versions of a Climate Model

Tomoo Ogura[1], Mark J. Webb[2], and Adrian P. Lock[2]

[1]National Institute for Environmental Studies, Tsukuba, Japan.

[2]Met Office Hadley Centre, Exeter, United Kingdom.

Corresponding author: Tomoo Ogura (ogura@nies.go.jp)

Key Points:

- The increase in longwave radiation from the sea surface is a leading order cause of the positive low cloud feedback in a climate model.
- This increase in longwave radiation leads to warming and drying in the boundary layer, which contributes to the decrease in the low cloud.
- This mechanism is not associated with increases in surface evaporation or vertical moisture contrast.

Abstract

Low cloud feedback in global warming projections by climate models is characterized by its positive sign, the mechanism of which is not well understood. Here we propose that the positive sign is primarily caused by the increase in upward longwave radiation from the sea surface. We devise numerical experiments that enable separation of the feedback into components coming from physically distinct causes. Results of these experiments with a climate model indicate that increases in upward longwave radiation from the sea surface cause warming and absolute drying in the boundary layer, leading to the positive low cloud feedback. The absolute drying results from decrease in surface evaporation, and also from decrease in inversion strength which enhances vertical mixing of drier free tropospheric air into the boundary layer. This mechanism is different from previously proposed understanding that positive low cloud feedback is caused by increases in surface evaporation or vertical moisture contrast.

Plain Language Summary

We project future climate change induced by atmospheric greenhouse gas increases by conducting numerical simulations using specialized computer codes, namely Global Climate Models. Results of such simulations are characterized by decreases in low cloud with warming at the Earth's surface, which amplifies the warming by reflecting less sunlight back to space and allowing more sunlight to be absorbed at the surface. This amplifying effect, called 'positive low cloud feedback', is important because the amount of future warming affects our living and safety. However, the mechanism of the low cloud decreases with warming is not well understood. Here we propose that the low cloud decrease is primarily caused by increase in upward longwave radiation from the sea surface. We devise numerical simulations that enable the separation of the low cloud feedback into components coming from physically distinct causes. Results of the simulations indicate that increases in upward longwave radiation from the sea surface cause warming and drying near the Earth's surface, leading to the low cloud decrease. This mechanism is different from previously proposed understanding that the low cloud decrease is due to increases in sea surface evaporation or vertical moisture contrast.

1 Introduction

Low cloud feedback is an important source of uncertainty in the projections of future climate using general circulation models (GCMs). The projections of future climate by multiple GCMs exhibit large inter-model differences, which cause difficulty in evaluating the impact of climate change. The inter-model difference in the projected surface air temperature for a given CO_2 increase is mainly attributable to the inter-model difference in cloud feedback (e.g., Caldwell et al. 2016; Vial et al. 2013; Webb et al. 2013). Specifically, changes in low cloud induced by surface warming make the largest contribution to this uncertainty (e.g., Zelinka et al. 2016, 2020). Understanding the inter-model difference in low cloud feedback is thus imperative, which motivates research on the mechanism of the low cloud feedback simulated by the GCMs.

An interesting feature of the low cloud feedback simulated by the GCMs is that it is positive in most models (Zelinka et al. 2020). The positive sign is associated with decreases in low cloud amount with surface warming, which amplifies the warming by allowing more solar radiation to be absorbed at the surface. However, the magnitude of the low cloud decrease varies widely across models, leading to a large uncertainty in the low cloud feedback. A critical question here is why low cloud decreases with surface warming, the mechanism of which is not well understood (Boucher et al. 2013; Forster et al. 2021).

Several studies have been conducted to address this issue by attributing simulated changes in low cloud to changes in environmental factors (Qu et al. 2014, 2015; Zhai et al. 2015; Myers and Norris 2016; Brient and Schneider 2016; McCoy et al. 2017; Klein et al. 2017). Qu et al. (2014), among others, developed a heuristic model which interprets the positive low cloud feedback in the subtropical low cloud regions in GCMs. The model indicates that changes in low cloud amount mainly come from two factors: local SST warming and increase in the strength of the inversion capping the atmospheric boundary layer, which is measured by the Estimated Inversion Strength (EIS, Wood and Bretherton 2006). The local SST warming tends to decrease low cloud, while the enhancement of EIS tends to increase the cloud. The net effect is a decrease in low cloud amount because the effect of the SST outweighs that of the EIS in most models.

The mechanism underlying the effect of EIS on low cloud is well understood (Klein and Hartmann 1993; Wood and Bretherton 2006). However, the mechanism of how the local SST warming influences the low cloud is still under debate. The following two mechanisms have been proposed, based on studies using Large Eddy Simulations. First, SST warming leads to an increase in surface latent heat flux, which enhances vertical mixing by turbulence or convection in the lower troposphere. This enhances entrainment of drier air from the free troposphere into the moister boundary layer, desiccating low cloud (Rieck et al. 2012). Second, the increase in latent heat flux from the sea surface induces an increase in water vapor specific humidity in the atmosphere. The magnitude of the increase in humidity is more pronounced in the boundary layer than in free troposphere, increasing the vertical moisture contrast. This increase in moisture contrast enhances the efficiency with which vertical mixing dehydrates the boundary layer, reducing low cloud (Bretherton and Blossey 2014, Sherwood et al. 2014, van der Dussen et al. 2015).

Recently, however, detailed examination of some GCM experiments gave results which are not consistent with the above understanding. For instance, Webb et al. (2018) explored the impact of surface latent heat flux on low cloud amount, forcing the latent heat flux to increase at different rates with SST warming in HadGEM2-A. They found that the magnitude of the low cloud decrease becomes smaller when the latent heat flux is forced to increase at higher rates. Similar results were obtained by Watanabe et al. (2018) using MIROC5. These findings suggest that mechanisms other than the increase in latent heat flux are needed to explain the decrease in low cloud with SST warming in climate models. However, such mechanisms are yet to be identified. Here we propose an alternative mechanism for the low cloud decrease with SST warming based on a new method for decomposing feedbacks in GCM experiments. We argue that the increase in upward longwave radiation from the sea surface is a leading order cause of the low cloud decrease.

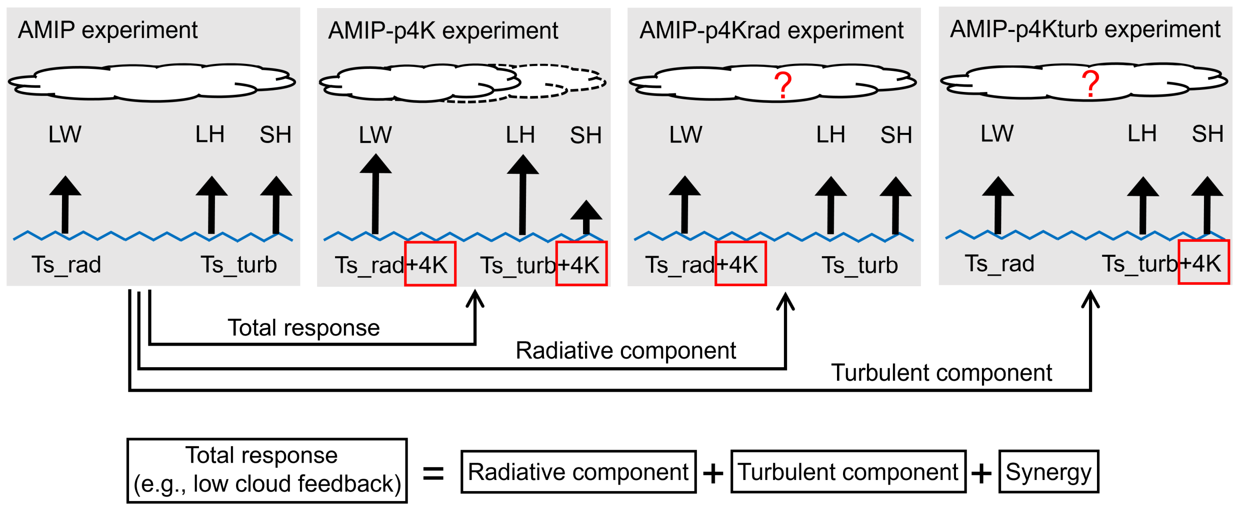

Figure 1. Schematic showing the experimental design. Ts_rad indicates the SST used for calculating LW radiation from the sea surface. Ts_turb is the SST used for calculating turbulent transport from the sea surface, including latent heat (LH) and sensible heat (SH) fluxes.

2 Numerical experiments

The low cloud feedback is investigated using an atmospheric GCM MIROC6 with the spatial resolution of T85 (~1.4˚) with 81 vertical levels (Tatebe et al. 2019). The simulation protocol follows that of the Atmospheric Model Intercomparison Project (AMIP), because the AMIP-type experiments can simulate the low cloud changes that are caused by the SST warming, which are the main focus of this study. They also provide a good approximation to the cloud feedbacks determined from coupled atmosphere-ocean CO_2-forced simulations (Ringer et al. 2014).

In the AMIP-p4K run, the uniform SST warming of 4K compared to the AMIP run modifies the atmosphere via two causal pathways, firstly by increasing the upward longwave radiation from the sea surface, and secondly by changing the turbulent transport at the air-sea interface, such as the latent and sensible heat fluxes (Figure 1). The decrease in low cloud amount, and hence the positive low cloud feedback, is a result of these two causal factors.

We attempt to better understand the roles of the two factors by adding two experiments. In the first experiment, SST is raised by 4K only when calculating the upward longwave radiation from the sea surface using Planck function (AMIP-p4Krad experiment, Figure 1). In the second, SST is raised by 4K only when calculating the turbulent transport at the air-sea interface using bulk aerodynamic formulas (AMIP-p4Kturb experiment). More details of the two experiments are given in the Supporting Information (Text S1). All of the experiments are integrated for 1979-2014 and the output is averaged for 36 years.

The differences of the SST warming experiments compared to the AMIP run are called 'total response (AMIP-p4K minus AMIP)', 'radiative component (AMIP-p4Krad minus AMIP)', and 'turbulent component (AMIP-p4Kturb minus AMIP)', respectively. As the total response, we focus on the low cloud feedback, and write it as a sum of the radiative component, the turbulent component, and a synergy term (Figure 1). Now the low cloud feedback is separated into components that originate from physically distinct causes, namely, the effect of increasing SST on upwelling surface longwave radiation and its effect on surface turbulent fluxes. The intention here is to see which component makes the low cloud feedback positive. The synergy is a residual term that is evaluated as the difference between the total response and the sum of the radiative and turbulent components. It represents the effect of the radiative and turbulent components working together.

All of the experiments, as outlined above, are repeated using another atmospheric GCM MIROC5 with the spatial resolution of T42 (~2.8˚) with 40 vertical levels (Shiogama et al. 2012; Ogura et al. 2017). In the following, however, we present the output of MIROC6 only, since the results from MIROC5 are similar to those from MIROC6. Results from MIROC5 are shown in the Supporting Information so that readers can confirm robustness of the conclusions (Figures S1-S3).

3 Results

We first present the low cloud feedback simulated by MIROC6 in Figure 2(a). This is evaluated by multiplying changes in the ISCCP low cloud amount by the cloud radiative kernel, which gives the changes in radiation flux at the TOA induced by the low cloud changes (Zelinka et al. 2012; Bodas-Salcedo et al. 2011; Klein and Jakob 1999; Webb et al. 2001). The ISCCP cloud amount with cloud top pressure greater than 680hPa is used for the evaluation. In Figure 2(a), we confirm that the global average low cloud feedback is positive. The positive signal is particularly evident in subtropical marine regions off the western coasts of continents, where low clouds prevail in both observations and model control climates.

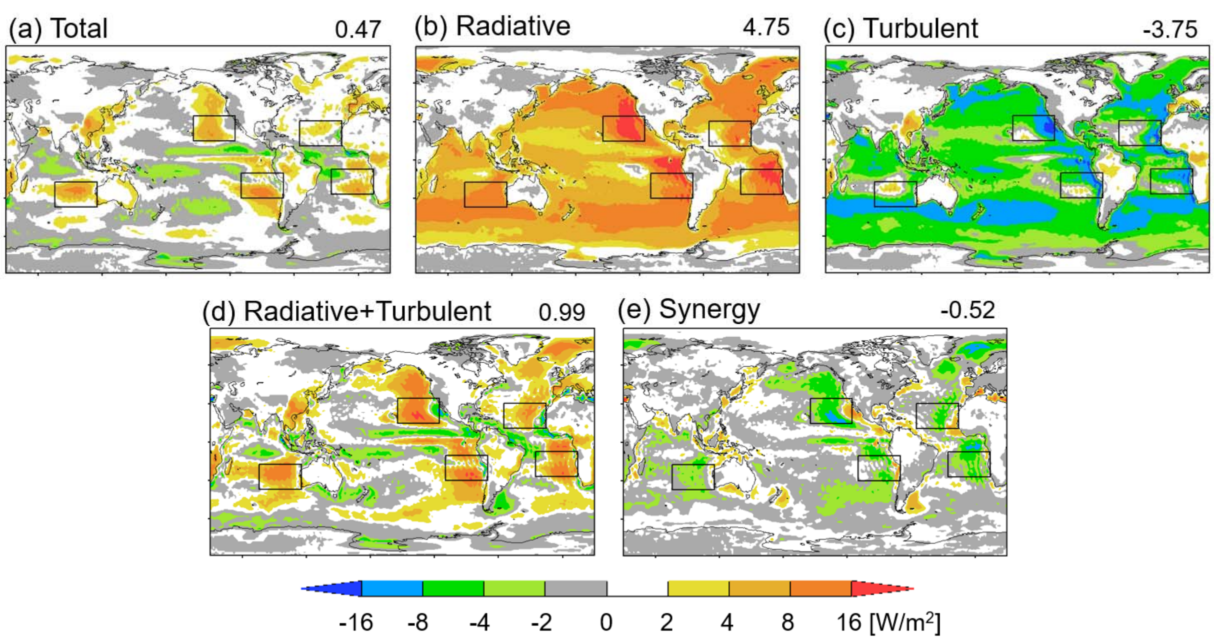

Figure 2. Low cloud feedback induced by 4K increases in SST. (a) Total low cloud feedback, (b) radiative component, (c) turbulent component, (d) sum of the radiative and turbulent components, and (e) synergy. Global averages are indicated at the top right of each panel. The

units can be converted to [$W/m^2/K$] by dividing by the surface warming of 4.54K in the AMIP-p4K run. Black rectangles indicate low cloud regions focused on in Figures 3 and 4.

The low cloud feedback is separated into the radiative component, turbulent component, and synergy as shown in Figure 2(b,c,e). The radiative component is characterized with positive contributions over the oceans, while the turbulent component is dominated by negative contributions (Figure 2b,c). If we add the two components together, as shown in Figure 2(d), the result captures the geographical pattern (especially the sign) of the total low cloud feedback in Figure 2(a). The pattern correlation between Figures 2(a) and 2(d) is 0.81. Therefore, the low cloud feedback can be approximated as a sum of the radiative and turbulent components, although the synergy effect is not negligible as shown in Figure 2(e).

Focusing on the sum of the radiative and the turbulent components in Figure 2(d), we find that the low cloud feedback becomes positive where the radiative component outweighs the turbulent component. Without the radiative component, the low cloud feedback would have been negative overall (Figure 2c). This means that the low cloud feedback becomes positive because of the radiative component. In other words, the positive sign of the feedback is mainly attributed to the increase in upward longwave radiation from the sea surface.

How does the longwave radiation cause the positive low cloud feedback? The mechanism is further examined, focusing on area averages over the five oceanic regions indicated by the black rectangles in Figure 2. These regions are chosen because the positive low cloud feedback stands out here in MIROC6 (Figure 2a), and also because they match the low cloud regions based on observations (Qu et al. 2014). Here, vertical profiles of cloud-related variables are examined in Figure 3. We focus on the cloud amount below the 680hPa level because this is where the low cloud feedback originates (Figure 3a,e). Note also that the low cloud feedback is strongly correlated with the cloud amount, but less well with the cloud optical thickness or cloud top pressure (Figure S4).

The total response of the cloud amount below the 680hPa level (Figure 3e, black) shows a characteristic dipole pattern, in which a cloud decrease above (σ-p level≈0.85) is moderated by a cloud increase below (σ-p level$\gtrsim$0.9). The dipole pattern reflects shallowing of the boundary layer cloud at σ-p level≈0.9 (Figure 3a). As a comparison, we also plot the radiative and turbulent components in Figure 3e (red and blue). Clearly, the turbulent component (blue) fails to reproduce the total response (black) at the σ-p level$\gtrsim$0.9, namely, the blue curve exceeds the black one. This explains how the turbulent component shows increase in low cloud, leading to the negative feedback. In contrast, the radiative component (red) shows a decrease in low cloud at σ-p level≈0.9, which opposes the cloud increase in the turbulent component (blue). When added together, the radiative and turbulent components (green) roughly reproduce the dipole pattern in the total response (black), although the positive and negative maxima are exaggerated. Hence, the low cloud decrease in the radiative component (red) is the key to understanding the low cloud decrease in the total response (black).

The low cloud decrease in the radiative component (Figure 3e, red) is consistent with a decrease in relative humidity (Figure 3f, red), which comes from both a warming and a decrease in specific humidity (Figure 3gh, red). This can be confirmed by looking at the geographical distribution (Figure S5). The warming is caused by the increase in upward longwave radiation from the sea surface, which is absorbed by the atmosphere (Figure 3i). The decrease in specific humidity can be explained by two mechanisms. Firstly, the magnitude of the warming is larger in the boundary layer compared to the free troposphere, having a bottom-heavy vertical profile (Figure 3h, red). This decreases the strength of the inversion capping the boundary layer. As a result, vertical mixing across the inversion increases, making the boundary layer less humid (Klein and Hartmann 1993). Secondly, the longwave-induced warming of the atmosphere increases the static stability at the air-sea interface. Note that the SST is kept the same as the AMIP experiment except for calculating the upward longwave radiation. The increase in the static stability suppresses the turbulent transport of water vapor from the sea surface (Text S2, Figure S9).

The warming and the absolute drying in the boundary layer, as described above, leads to the low cloud decrease in the radiative component. The mechanism may be summarized as "Cloud Reduction due to Increased Surface Temperature Longwave Emission (CRISTLE)". In addition, the decrease in the low cloud initiates a process that reduces the low cloud further. Namely, the decrease in the low cloud causes weakening of the radiative cooling of the boundary layer (Figure S8d,f, black). This contributes to warming and a decrease in relative humidity, thereby reducing the low cloud further (Figure S7e, green, Brient and Bony 2012). We note that the low cloud decrease in the radiative component is not associated with an increase in specific humidity or surface evaporation (Figures 3g, S9a). We also considered a number of other possible explanations for the low cloud reductions in the radiative component (Table S1).

In the turbulent component, by contrast, the low cloud changes are associated with the increase in specific humidity and surface evaporation. We attribute the low cloud increases in the turbulent component to multiple processes that compete with each other, as in Vial et al. (2016). For instance, the magnitude of the increase in specific humidity is larger at lower altitudes, which enhances the moisture contrast between the free troposphere and the boundary layer (Figure 3g, blue). As a result, the upward moisture flux by shallow convection increases, which tends to decrease the low cloud (Figures S6c,f, red, Zhang et al. 2013). In contrast, we also note that the vertical temperature profile stabilizes with warming, which increases strength of the inversion capping the boundary layer (Figure 3h, blue). As a result, vertical mixing across the inversion reduces, which tends to keep the boundary layer more humid and increase the low cloud (Miller 1997). Understanding the roles of different processes within the turbulent component will be a subject of future studies. More details of the competing processes are given in Table S1.

The results obtained so far illustrate how the low cloud feedback originates from the sea surface warming. The processes involved in the feedback are classified into the radiative and the turbulent components. The two components are dissimilar to each other, with the former decreasing the ISCCP low cloud amount (LCA), while the latter increases it. However, the two components are both related to changes in the EIS, as follows. In the radiative component, the LCA decreases as the EIS decreases (Figure 3e,h, red). In the turbulent component, the LCA increases as the EIS increases (Figure 3e,h, blue). In the synergy component, also, the LCA increases as the EIS increases (not shown). The relationship between the LCA and the EIS is qualitatively consistent with observation (Wood and Bretherton 2006; Klein and Hartmann 1993).

If we add the three components together, however, the relation between the LCA and the EIS changes compared to that above. Namely, the LCA decreases as the EIS increases (Figure

3e,h, black), which may appear counter-intuitive. Why does the relation between the LCA and the EIS break down when the components are added together? This issue is examined in Figure 4(a).

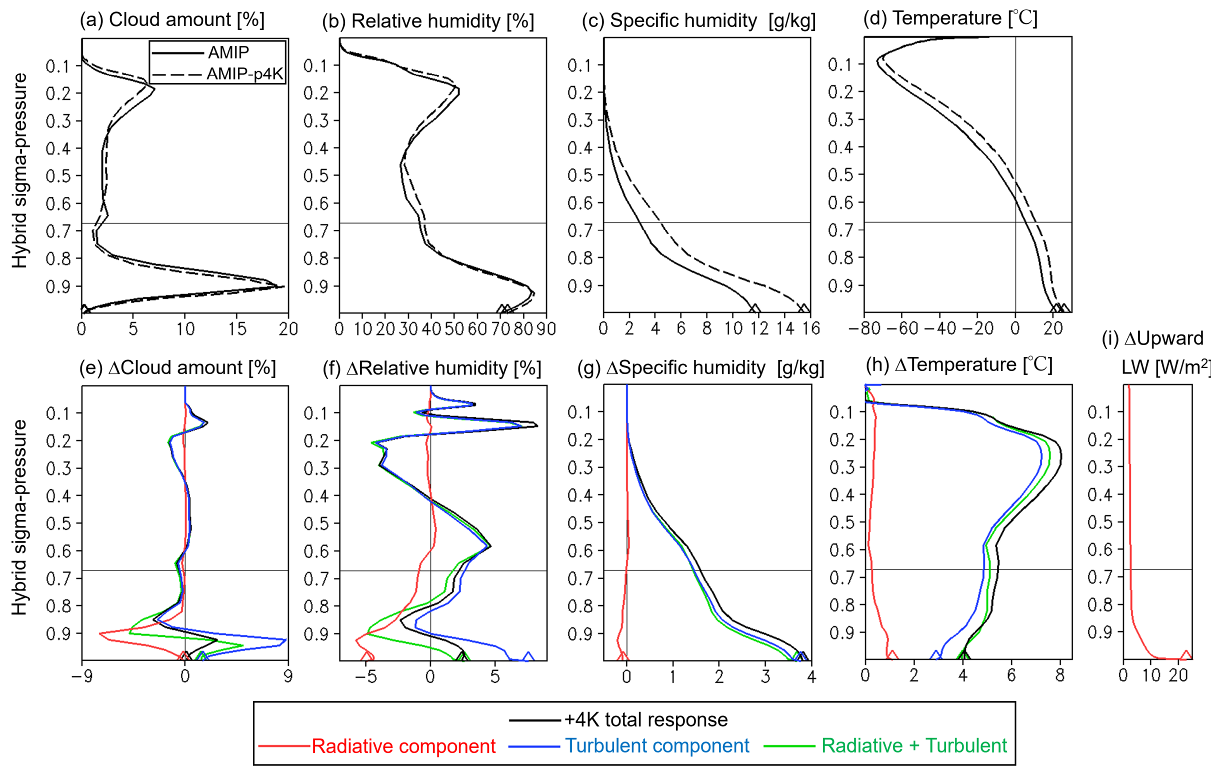

Figure 3. Vertical profiles of cloud-related variables averaged over the low cloud regions indicated by the black rectangles in Figure 2. (a)(b)(c)(d) for AMIP and AMIP-p4K experiments, and (e)(f)(g)(h)(i) for changes due to +4K SST warming. The vertical coordinate is hybrid σ-p on model level. Horizontal lines at the σ-p level of 0.67 mark the boundary between low-top clouds and middle-top clouds at 680hPa. Diamonds indicate values at the lowest level. The changes in upward longwave, (i), are evaluated assuming that the atmosphere remains fixed at the AMIP condition.

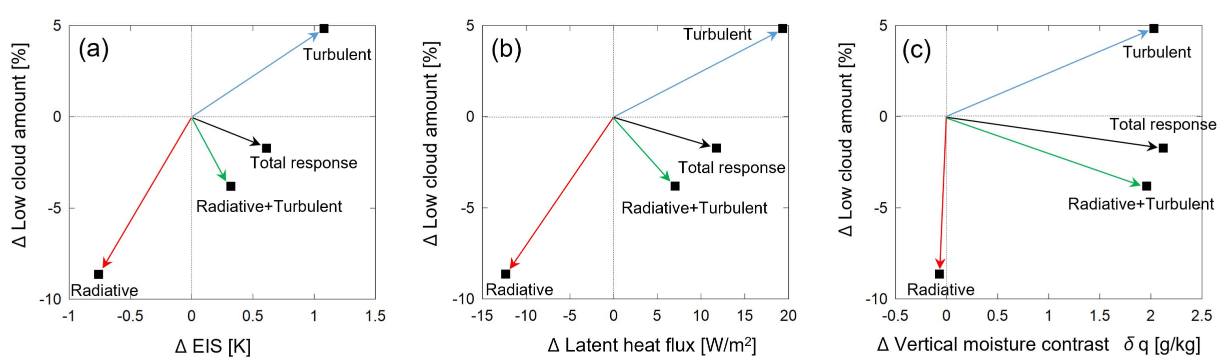

Figure 4 Relationships between changes in low cloud amount and changes in (a) EIS, (b) latent heat flux, and (c) vertical moisture contrast δ q. The δ q is defined as the specific humidity q at 1000hPa minus q at 700 hPa. The delta, Δ, denotes changes induced by the SST warming of 4K. The data are averages over the low cloud regions indicated by the black rectangles in Figure 2.

In figure 4(a), the changes induced by the SST warming of 4K are represented by 2-D vectors on the ΔEIS-ΔLCA plane. The radiative component is shown in red, with the coordinate values of $(\Delta EIS_{rad}, \Delta LCA_{rad})$, while the turbulent component is shown by blue, with the coordinate values of $(\Delta EIS_{turb}, \Delta LCA_{turb})$. The two vectors appear in the 3rd and the 1st quadrants, indicating that the LCA decreases (increases) as the EIS decreases (increases). Adding the two components together, we obtain the sum shown by green, with the coordinate values of $(\Delta EIS_{turb} + \Delta EIS_{rad}, \Delta LCA_{turb} + \Delta LCA_{rad})$. Now the vector appears in the 4th quadrant, indicating that the LCA decreases as the EIS increases, which captures the sign of the total response shown in black.

Focusing on the sum of the two components, we find that the LCA decreases as the EIS increases under the following conditions:

$$\Delta EIS_{turb} + \Delta EIS_{rad} > 0\ , and\ \Delta LCA_{turb} + \Delta LCA_{rad} < 0 \qquad (1).$$

Namely, the change in the EIS is dominated by the turbulent component, while the change in the LCA is dominated by the radiative component. In other words, the total response to the SST warming includes two counter-acting components, and which component dominates depends on the variable we look at. This explains how the relation between the LCA and the EIS changes when adding the radiative and turbulent components together.

We also note that rate of change in the LCA with respect to the EIS is different between the radiative and turbulent components, as follows:

$$\Delta LCA_{rad}/\Delta EIS_{rad} > \Delta LCA_{turb}/\Delta EIS_{turb} \qquad (2).$$

The conditions (1) can be met only under the condition (2). The condition (2) indicates that LCA is less sensitive to EIS in the turbulent component than in the radiative component. This may be because, in the turbulent component, the EIS increase is accompanied by an increase in vertical moisture contrast, δ q (Figure 3gh, blue). The change in the EIS tends to increase the LCA, while the change in the δ q tends to decrease it, making the LCA less sensitive to the EIS (Kawai et al. 2017).

Similar arguments hold, even if we replace the EIS with the surface latent heat flux or the vertical moisture contrast, δ q (Figure 4b,c). Namely, in the total response shown in black, the LCA decrease is accompanied by an increase in latent heat flux or δ q. This can be explained by the fact that the LCA decrease is dominated by the radiative component while the increase in latent heat flux or δ q is driven by the turbulent component.

4 Conclusions

In order to understand the reason for the positive sign of the low cloud feedback simulated by GCMs, we devise numerical experiments which enable separation of the feedback into a component driven by upward surface longwave radiation and another driven by surface turbulent fluxes. The numerical experiments are conducted using MIROC5 and MIROC6. The results indicate that the positive sign of the low cloud feedback is mainly attributed to the increase in longwave radiation from the sea surface, which leads to a warming and a drying in the boundary layer, as well as a decrease in the low cloud amount (LCA). The mechanism involved is summarized as "Cloud Reduction due to Increased Surface Temperature Longwave Emission (CRISTLE)". It is not associated with increases in surface latent heat flux or vertical moisture contrast. The decomposition of the feedback also helps to explain how the LCA decrease is accompanied by increases in the EIS, the latent heat flux, and the vertical moisture contrast.

In addition, the obtained results indicate that changes in the turbulent fluxes tend to increase the LCA, thereby making the feedback more negative in MIROC5 and MIROC6. The results are consistent with the idea that changes in the turbulent fluxes are an important factor that controls the low cloud feedback. The cloud feedback is affected by changes in the turbulent fluxes in remote regions as well as the changes below the low clouds. Indeed, the changes in the turbulent fluxes and the upward surface longwave radiation are both needed to explain the geographical pattern of the low cloud feedback.

Whether other GCMs or Large Eddy Simulations support the present findings will be an interesting topic for future studies. Currently, output from CMIP6 experiments is analyzed to see if the mechanism proposed in this study can explain the sub-tropical low cloud feedbacks in multi-GCMs. In addition, the experiments proposed in this study are being conducted with Large Eddy Simulations under the CGILS protocol (Blossey et al. 2016). The results will be presented in subsequent papers.

Acknowledgments

This study was funded by the Integrated Research Program for Advancing Climate Models (Grant Number JPMXD0717935457) and the Program for the Advanced Studies of Climate Change Projection (Grant Number JPMXD0722680395) from the Ministry of Education, Culture, Sports, Science and Technology, Japan. Mark Webb was funded by the UK BEIS/Defra Met Office Hadley Centre Climate Programme (GA01101). Simulations were performed with the NIES supercomputer system and the Earth Simulator at JAMSTEC. We thank Mark D. Zelinka for providing cloud radiative kernel, and Tokuta Yokohata and Koji Ogochi for implementing COSP in MIROC5. Figures in this paper were plotted using Grid Analysis and Display System (GrADS). Data used in this study are archived at https://doi.org/10.5281/zenodo.4153249.

References

Blossey, P. N., C. S. Bretherton, A. Cheng, S. Endo, T. Heus, A. P. Lock, and J. J. van der Dussen (2016), CGILS Phase 2 LES intercomparison of response of subtropical marine low cloud regimes to CO_2 quadrupling and a CMIP3 composite forcing change, *J. Adv. Model. Earth Syst.*, 08, doi:10.1002/2016MS000765.

Boucher, O., D. Randall, P. Artaxo, C. Bretherton, G. Feingold, P. Forster, V. -M. Kerminen, Y. Kondo, H. Liao, U. Lohmann, P. Rasch, S. K. Satheesh, S. Sherwood, B. Stevens, and X. Y. Zhang (2013), Clouds and Aerosols. In:*Climate Change 2013:The Physical Science Basis. Contribution of Working Group 1 to the Fifth Assessment Report of the Intergovernmental Panel on Climate Change* [Stocker, T. F., D. Qin, G. -K. Plattner, M. Tignor, S. K. Allen, J. Boschung, A. Nauels, Y. Xia, V. Bex, and P. M. Midgley (eds.)]. Cambridge University Press, Cambridge, United Kingdom and New York, NY, USA.

Bodas-Salcedo, A., M. J. Webb, S. Bony, H. Chepfer, J. -L. Dufresne, S. A. Klein, Y. Zhang, R. Marchand, J. M. Haynes, R. Pincus, and V. O. John (2011), COSP Satellite simulation software for model assessment, *Bull. Amer. Meteor. Soc.*, 92, 1023–1043, doi:10.1175/2011BAMS2856.1.

Bretherton, C. S. and P. N. Blossey (2014), Low cloud reduction in a greenhouse-warmed climate: Results from Lagrangian LES of a subtropical marine cloudiness transition, *J. Adv. Model. Earth Syst*., 6, doi:10.1002/2013MS000250.

Brient, F. and S. Bony (2012), How may low-cloud radiative properties simulated in the current climate influence low-cloud feedbacks under global warming? *Geophys. Res. Lett.*, 39, L20807, doi:10.1029/2012GL053265.

Brient, F. and T. Schneider (2016), Constraints on climate sensitivity from space-based measurements of low-cloud reflection, *J. Clim.*, 29, 5821–5835, doi:10.1175/JCLI-D-15-0897.1.

Caldwell, P. M., M. D. Zelinka, K. E. Taylor and K. Marvel (2016), Quantifying the sources of intermodal spread in equilibrium climate sensitivity, *J. Clim.*, 29, 513–524, doi:10.1175/JCLI-D-15-0352.1.

Forster, P., T. Storelvmo, K. Armour, W. Collins, J.-L. Dufresne, D. Frame, D. J. Lunt, T. Mauritsen, M. D. Palmer, M. Watanabe, M. Wild, and H. Zhang (2021), The Earth's Energy Budget, Climate Feedbacks, and Climate Sensitivity. In *Climate Change 2021: The Physical Science Basis. Contribution of Working Group 1 to the Sixth Assessment Report of the Intergovernmental Panel on Climate Change* [Masson-Delmotte, V., P. Zhai, A. Pirani, S. L. Connors, C. Péan, S. Berger, N. Caud, Y. Chen, L. Goldfarb, M. I. Gomis, M. Huang, K. Leitzell, E. Lonnoy, J. B. R. Matthews, T. K. Maycock, T. Waterfield, O. Yelekçi, R. Yu, and B. Zhou (eds.)]. Cambridge University Press, Cambridge, United Kingdom and New York, NY, USA, pp.923-1054, doi:10.1017/9781009157896.009.

Kawai, H., T. Koshiro, and M. J. Webb (2017), Interpretation of factors controlling low cloud cover and low cloud feedback using a unified predictive index, *J. Clim.*, 30, 9119-9131, doi:10.1175/JCLI-D-16-0825.1.

Klein, S. A., and D. L. Hartmann (1993), The seasonal cycle of low stratiform clouds, *J. Clim.*, 6, 1587–1606.

Klein, S. A., and C. Jakob (1999), Validation and sensitivities of frontal clouds simulated by the ECMWF model, *Mon. Wea. Rev.*, 127, 2514–2531.

Klein, S. A., A. Hall, J. R. Norris, and R. Pincus (2017), Low-cloud feedbacks from cloud-controlling factors: a review, *Surv. Geophys.*, 38, 1307–1329, doi:10.1007/s10712-017-9433-3.

McCoy, D. T., R. Eastman, D. L. Hartmann, and R. Wood (2017), The change in low cloud cover in a warmed climate inferred from AIRS, MODIS, and ERA-Interim, *J. Clim.*, 30, 3609-3620, doi:10.1175/JCLI-D-15-0734.1.

Miller, R. L. (1997), Tropical thermostats and low cloud cover, *J. Clim.,* 10, 409-440.

Myers, T. A., and J. R. Norris (2016), Reducing the uncertainty in subtropical cloud feedback, *Geophys. Res. Lett.*, 43, doi:10.1002/2015GL067416.

Narenpitak, P., and C. S. Bretherton (2019), Understanding negative subtropical shallow cumulus cloud feedbacks in a near-global aquaplanet model using limited area cloud-resolving simulations, *J. Adv. Model. Earth Syst.,* 11, 1600-1626, doi:10.1029/2018MS001572.

Ogura, T., H. Shiogama, M. Watanabe, M. Yoshimori, T. Yokohata, J. D. Annan, J. C. Hargreaves, N. Ushigami, K. Hirota, Y. Someya, Y. Kamae, H. Tatebe, and M. Kimoto (2017), Effectiveness and limitations of parameter tuning in reducing biases of top-of-atmosphere radiation and clouds in MIROC version 5, *Geosci. Model Dev.*, 10, 4647-4664, doi:10.5194/gmd-10-4647-2017.

Qu, X., A. Hall, S. A. Klein, and P. M. Caldwell (2014), On the spread of changes in marine low cloud cover in climate model simulations of the 21st century, *Clim. Dyn.*, 42, 2603–2626, doi:10.1007/s00382-013-1945-z.

Qu, X., A. Hall, S. A. Klein, and A. M. DeAngelis (2015), Positive tropical marine low-cloud cover feedback inferred from cloud-controlling factors, *Geophys. Res. Lett.*, 42, 7767–7775, doi:10.1002/2015GL065627.

Rieck, M., L. Nuijens, and B. Stevens (2012), Marine boundary layer cloud feedbacks in a constant relative humidity atmosphere, *J. Atmos. Sci.*, 69, 2538–2550, doi:10.1175/JAS-D-11-0203.1.

Ringer, M. A., T. Andrews, and M. J. Webb (2014), Global-mean radiative feedbacks and forcing in atmosphere-only and coupled atmosphere-ocean climate change experiments, *Geophys. Res. Lett.,* 41, doi:10.1002/2014GL060347.

Sherwood, S. C., S. Bony, and J. -L. Dufresne (2014), Spread in model climate sensitivity traced to atmospheric convective mixing, *Nature*, 505, 37–42, doi:10.1038/nature12829.

Shiogama, H., M. Watanabe, M. Yoshimori, T. Yokohata, T. Ogura, J. D. Annan, J. C. Hargreaves, M. Abe, Y. Kamae, R. O'ishi, R. Nobui, S. Emori, T. Nozawa, A. Abe-Ouchi, and M. Kimoto (2012), Perturbed physics ensemble using the MIROC5 coupled atmosphere-ocean GCM without flux corrections: experimental design and results -parametric uncertainty of climate sensitivity, *Clim. Dyn.*, 39, 3041–3056, doi:10.1007/s00382-012-1441-x.

Tatebe, H., T. Ogura, T. Nitta, Y. Komuro, K. Ogochi, T. Takemura, K. Sudo, M. Sekiguchi, M. Abe, F. Saito, M. Chikira, S. Watanabe, M. Mori, N. Hirota, Y. Kawatani, T. Mochizuki, K. Yoshimura, K. Takata, R. O'ishi, D. Yamazaki, T. Suzuki, M. Kurogi, T. Kataoka, M. Watanabe, and M. Kimoto (2019), Description and basic evaluation of simulated mean state, internal variability, and climate sensitivity in MIROC6, *Geosci. Model Dev.*, 12, 2727–2765, doi:10.5194/gmd-12-2727-2019.

van der Dussen, J. J., S. R. de Roode, S. Dal Gesso, and A. P. Siebesma (2015), An LES model study of the influence of the free tropospheric thermodynamic conditions on the stratocumulus response to a climate perturbation, *J. Adv. Model. Earth Syst.*, 7, 670–691, doi:10.1002/2014MS000380.

Vial, J., J. -L. Dufresne, and S. Bony (2013), On the interpretation of inter-model spread in CMIP5 climate sensitivity estimates, *Clim. Dyn.*, 41, 3339–3362, doi:10.1007/s00382-013-1725-9.

Vial, J., S. Bony, J.-L. Dufresne, and R. Roehrig (2016), Coupling between lower-tropospheric convective mixing and low-level clouds: Physical mechanisms and dependence on convection scheme, *J. Adv. Model. Earth Syst.*, 8, 1892-1911, doi:10.1002/2016MS000740.

Watanabe, M., T. Suzuki, R. O'ishi, Y. Komuro, S. Watanabe, S. Emori, T. Takemura, M. Chikira, T. Ogura, M. Sekiguchi, K. Takata, D. Yamazaki, T. Yokohata, T. Nozawa, H. Hasumi, H. Tatebe, and M. Kimoto (2010), Improved climate simulation by MIROC5: mean states, variability, and climate sensitivity, *J. Clim.*, 23, 6312–6335, doi:10.1175/2010JCLI3679.1.

Watanabe, M., Y. Kamae, H. Shiogama, A. M. DeAngelis, and K. Suzuki (2018), Low clouds link equilibrium climate sensitivity to hydrological sensitivity, *Nat. Clim. Change*, 8, 901–906, doi:10.1038/s41558-018-0272-0.

Webb, M. J., C. Senior, S. Bony, and J. -J. Morcrette (2001), Combining ERBE and ISCCP data to assess clouds in the Hadley Centre, ECMWF, and LMD atmospheric climate models, *Clim. Dyn.*, 17, 905–922.

Webb, M. J., F. Hugo Lambert, and J. M. Gregory (2013), Origins of differences in climate sensitivity, forcing and feedback in climate models, *Clim. Dyn.*, 40, 677–707, doi:10.1007/s00382-012-1336-x.

Webb, M. J., A. P. Lock, and F. Hugo Lambert (2018), Interactions between hydrological sensitivity, radiative cooling, stability, and low-level cloud amount feedback, *J. Clim.*, 31, 1833–1850, doi:10.1175/JCLI-D-16-0895.1.

Wood, R., and C. S. Bretherton (2006), On the relationship between stratiform low cloud cover and lower-tropospheric stability, *J. Clim.*, 19, 6425–6432, doi:10.1175/JCLI3988.1.

Wyant, M. C., C. S. Bretherton, and P. N. Blossey (2009), Subtropical low cloud response to a warmer climate in a superparameterized climate model. Part 1: Regime sorting and physical mechanisms, *J. Adv. Model. Earth Syst.,* 1, 7, doi:10.3894/JAMES.2009.1.7.

Zhai, C., J. H. Jiang, and H. Su (2015), Long-term cloud change imprinted in seasonal cloud variation: More evidence of high climate sensitivity, *Geophys. Res. Lett.*, 42, 8729-8737, doi:10.1002/2015GL065911.

Zhang, M., C. S. Bretherton, P. N. Blossey, P. H. Austin, J. T. Bacmeister, S. Bony, F. Brient, S. K. Cheedela, A. Cheng, A. D. Del Genio, S. R. De Roode, S. Endo, C. N. Franklin, J.-C. Golaz, C. Hannay, T. Heus, F. A. Isotta, J.-L. Dufresne, I.-S. Kang, H. Kawai, M. Köehler, V. E. Larson, Y. Liu, A. P. Lock, U. Lohmann, M. F. Khairoutdinov, A. M. Molod, R. A. J. Neggers, P. Rasch, I. Sandu, R. Senkbeil, A. P. Siebesma, C. Siegenthaler-Le Drian, B. Stevens, M. J. Suarez, K.-M. Xu, K. von Salzen, M. J. Webb, A. Wolf, and M. Zhao (2013), CGILS: Results from the first phase of an international project to understand the physical mechanisms of low cloud feedbacks in single column models, *J. Adv. Model. Earth Syst.*, 5, 1-17, doi:10.1002/2013MS000246.

Zelinka, M. D., S. A. Klein, and D. L. Hartmann (2012), Computing and partitioning cloud feedbacks using cloud property histograms. Part I:cloud radiative kernels, *J. Clim.*, 25, 3715-3735, doi:10.1175/JCLI-D-11-00248.1.

Zelinka, M. D., C. Zhou, and S. A. Klein (2016), Insights from a refined decomposition of cloud feedbacks, *Geophys. Res. Lett.*, 43, doi:10.1002/2016GL069917.

Zelinka, M. D., T. A. Myers, D. T. McCoy, S. Po-Chedley, P. M. Caldwell, P. Ceppi, S. A. Klein, and K. E. Taylor (2020), Causes of higher climate sensitivity in CMIP6 models. *Geophys. Res. Lett.*, 47, e2019GL085782. doi:10.1029/2019GL085782.

Figure 1.


AMIP experiment
LW
LH
SH
Ts_rad
Ts_turb
AMIP-p4K experiment
LW
LH
SH
Ts_rad+4K
Ts_turb+4K
AMIP-p4Krad experiment
?
LW
LH
SH
Ts_rad+4K
Ts_turb
AMIP-p4Kturb experiment
?
LW
LH
SH
Ts_rad
Ts_turb+4K
Total response
Radiative component
Turbulent component
Total response
(e.g., low cloud feedback)
=
Radiative component
+
Turbulent component
+
Synergy

Figure 2.

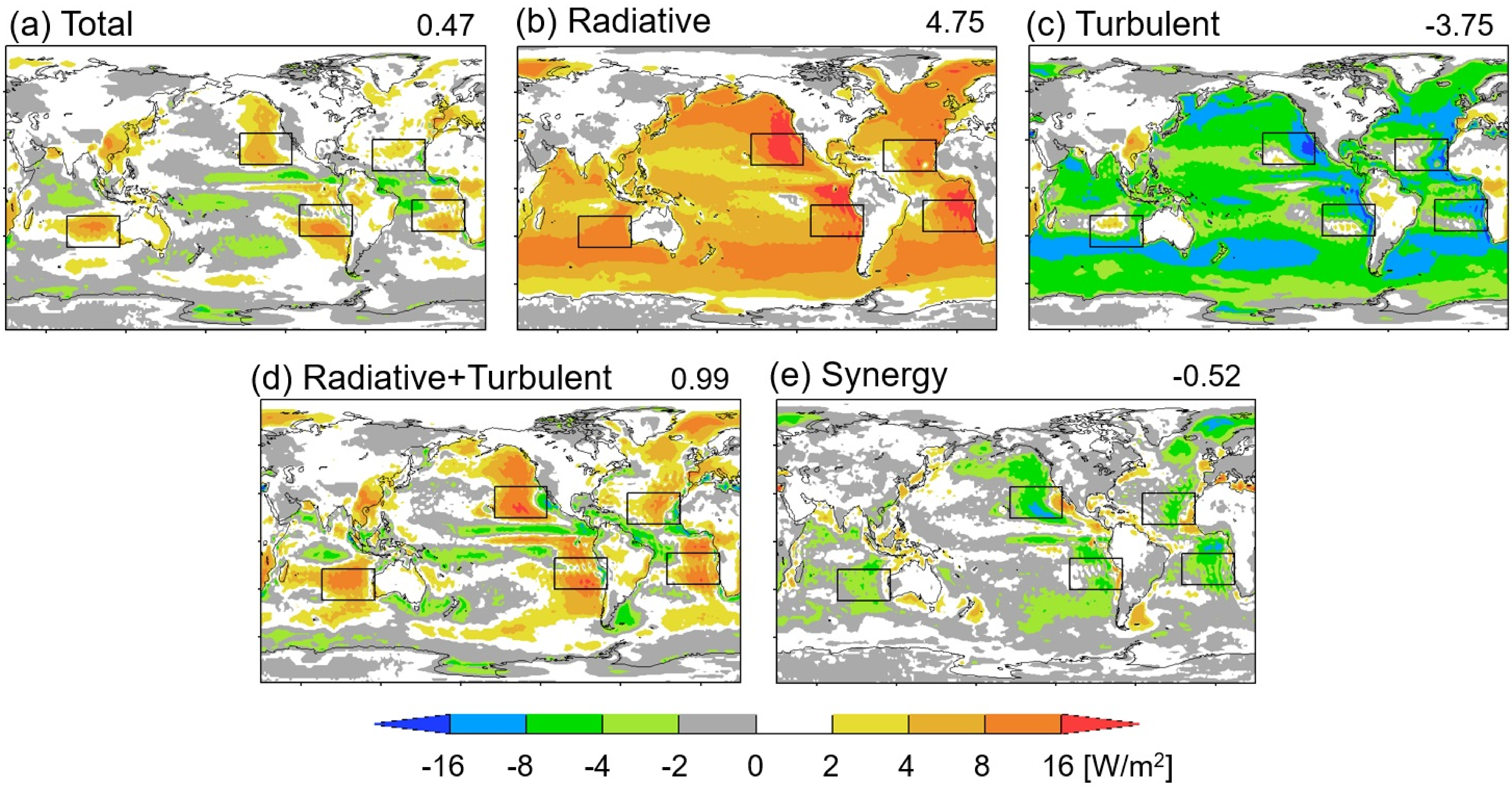

(a) Total
0.47
(b) Radiative
4.75
(c) Turbulent
-3.75
(d) Radiative+Turbulent
0.99
(e) Synergy
-0.52
-16
-8
-4
-2
0
2
4
8
16 [W/m2]

Figure 3.

(a) Cloud amount [%]
AMIP
AMIP-p4K
(b) Relative humidity [%]
(c) Specific humidity [g/kg]
(d) Temperature [℃]
Hybrid sigma-pressure
(e) ΔCloud amount [%]
(f) ΔRelative humidity [%]
(g) ΔSpecific humidity [g/kg]
(h) ΔTemperature [℃]
(i) ΔUpward LW [W/m²]
+4K total response
Radiative component
Turbulent component
Radiative + Turbulent

Figure 4.


(a)
Turbulent
Total response
Radiative+Turbulent
Radiative
Δ Low cloud amount [%]
Δ EIS [K]
(b)
Turbulent
Total response
Radiative+Turbulent
Radiative
Δ Low cloud amount [%]
Δ Latent heat flux [W/m2]
(c)
Turbulent
Total response
Radiative+Turbulent
Radiative
Δ Low cloud amount [%]
Δ Vertical moisture contrast δ q [g/kg]

AGU PUBLICATIONS

Geophysical Research Letters

Supporting Information for

Positive Low Cloud Feedback Primarily Caused by Increasing Longwave Radiation from the Sea Surface in Two versions of a Climate Model

Tomoo Ogura[1], Mark J. Webb[2], and Adrian P. Lock[2]

[1]National Institute for Environmental Studies, Tsukuba, Japan

[2]Met Office Hadley Centre, Exeter, United Kingdom

Contents of this file

Texts S1, S2, Figures S1, S2, S3, S4, S5, S6, S7, S8, S9, Table S1

Introduction

This document contains additional text, figures, and a table which support arguments in the main text.

Text S1. Experimental design

In MIROC5 and MIROC6, SST warming influences the atmosphere through changes in two factors. One is the upward longwave radiation emitted from the sea surface, and the other is the turbulent transport of heat, moisture, momentum, and aerosol from the sea surface. Without any changes in the two factors, the SST warming cannot influence the model atmosphere.

In the AMIP-p4K experiment, the SST warming changes both the two factors to influence the atmosphere. In the AMIP-p4Krad or the AMIP-p4Kturb experiment, the SST warming changes either one of the two factors to influence the atmosphere. Here we describe how the AMIP-p4Krad and AMIP-p4Kturb experiments are implemented.

1. AMIP-p4Krad experiment

In MIROC5 and MIROC6, upward longwave radiation that is emitted from the surface of the land or ocean is calculated from the surface temperature, T_{s_rad}, using Planck's function. This upward longwave radiation causes heating at multiple atmospheric layers above the surface.

In the AMIP experiment, we prescribe SST as a boundary condition, which is used as the input variable T_{s_rad} to calculate the upward longwave radiation emitted from the sea surface. In the AMIP-p4Krad experiment, we add 4K to the T_{s_rad} at the sea surface. The experimental setting of the AMIP-p4Krad is the same as the AMIP, other than adding 4K to the T_{s_rad}.

The 4K warming of T_{s_rad} causes an increase in upward longwave radiation emitted from the sea surface, which leads to an increase in radiative heating at multiple atmospheric layers above the surface (Figure 3i). As a result, the atmospheric temperature increases, which is prominent in the lower troposphere (red curve in Figure 3h).

2. AMIP-p4Kturb experiment

Turbulent transport of sensible heat, latent heat, and momentum from the surface to the atmosphere is calculated using the bulk aerodynamic formulas in the MIROC5 and MIROC6. The formulas are defined as follows.

$$SH = \rho \cdot C_p \cdot C_{DH}(T_{s\_turb}) \cdot |\vec{V}| \cdot \{T_{s\_turb} - T_a \cdot (P_s/P_a)^{R_{air}/C_p}\} \quad (1)$$

$$LE = \rho \cdot L_v \cdot C_{DE}(T_{s\_turb}) \cdot |\vec{V}| \cdot \{Q_{sat}(T_{s\_turb}) - Q_a\} \quad (2)$$

$$F_u = -\rho \cdot C_{DM}(T_{s\_turb}) \cdot |\vec{V}| \cdot U_a \quad (3)$$

$$F_v = -\rho \cdot C_{DM}(T_{s\_turb}) \cdot |\vec{V}| \cdot V_a \quad (4)$$

T_{s_turb} is surface temperature, SH is sensible heat flux, LE is latent heat flux, F_u and F_v are momentum fluxes, ρ is air density, C_p is specific heat of air at constant pressure, L_v is latent heat of condensation, $C_{DH}(T_{s\_turb})$, $C_{DE}(T_{s\_turb})$, and $C_{DM}(T_{s\_turb})$ are aerodynamic transfer coefficients that are dependent on T_{s_turb}, $|\vec{V}|$ is surface wind speed, T_a is temperature at the lowest atmospheric layer, P_s is surface pressure, P_a is pressure at the lowest atmospheric layer, R_{air} is the gas constant of air, $Q_{sat}(T_{s\_turb})$ is saturation specific humidity that is dependent on T_{s_turb}, Q_a is specific humidity at the lowest atmospheric layer, U_a is westerly wind speed at the lowest atmospheric layer, V_a is southerly wind speed at the lowest atmospheric layer.

The turbulent fluxes, SH, LE, F_u, and F_v, are dependent on T_{s_turb}. Likewise, the turbulent transport of aerosol from the surface to the atmosphere is also dependent on T_{s_turb}. In the AMIP experiment, SST is used as an input variable T_{s_turb} to calculate the turbulent transport of sensible heat, latent heat, momentum, and aerosol from the sea surface. In the AMIP-p4Kturb experiment, we add 4K to T_{s_turb} at the sea surface. The experimental setting of the AMIP-p4Kturb is the same as the AMIP, other than adding 4K to T_{s_turb}. The 4K warming of T_{s_turb} causes an increase in SH and LE. As a result, both atmospheric temperature and specific humidity increase (blue curves in Figure 3gh).

Text S2. Response of latent heat flux to increasing longwave radiation from the sea surface

In AMIP-p4Krad experiment, upward longwave radiation from the sea surface increases relative to the AMIP experiment, which leads to a reduction in the surface latent heat flux, as shown in Figure S9(a). The decrease in the surface latent heat flux contributes to the decrease in specific humidity (Figure 3g, red). To better understand the mechanism of the decrease in surface latent heat flux, we decompose the response of the surface latent heat flux into contribution from multiple factors, as follows.

In MIROC5 and MIROC6, the latent heat flux is calculated according to the equation (2) in Text S1. Time-averaging the equation (2), and focusing on the difference between AMIP-p4Krad and AMIP experiments, we obtain

$$\Delta\overline{LE} = L_v \cdot \Delta\overline{\rho \cdot |\vec{V}| \cdot C_{DE}(T_{s\_turb}) \cdot DELQ} \qquad (5)$$

where $DELQ \equiv Q_{sat}(T_{s\_turb}) - Q_a$, $\overline{(\quad)}$ is time-averaging, and Δ denotes AMIP-p4Krad minus AMIP experiment. We further rewrite the equation as

$$\Delta\overline{LE} = L_v \cdot \Delta\left\{\bar{\rho} \cdot \overline{|\vec{V}|} \cdot \overline{C_{DE}(T_{s\_turb})} \cdot \overline{DELQ}\right\} + residual \quad (6).$$

The magnitude of the residual in (6) depends on the period of time-averaging. Over the low latitude oceans it is mostly of the order of 10 W/m^2 for monthly, 0.5 W/m^2 for daily, and 0.1 W/m^2 for 6 hourly averages. In the following, we use daily averaged data so that the residual in (6) becomes much smaller than $\Delta\overline{LE}$, that is greater than 4 W/m^2 in magnitude (Figure S9(a)). Neglecting the residual, we assume that the equation (6) can be approximated as

$$\Delta\overline{LE} \approx L_v \cdot \Delta\left\{\bar{\rho} \cdot \overline{|\vec{V}|} \cdot \overline{C_{DE}(T_{s\_turb})} \cdot \overline{DELQ}\right\} \qquad (7).$$

Using the 1st Taylor polynomial, the right hand side of (7) can be written as,

$$\begin{aligned}\Delta\overline{LE} \approx\ & L_v \cdot \left\{\overline{|\vec{V}|} \cdot \overline{C_{DE}(T_{s_{turb}})} \cdot \overline{DELQ}\right\}_{AMIP} \cdot \Delta\bar{\rho} \\ & + L_v \cdot \left\{\bar{\rho} \cdot \overline{C_{DE}(T_{s_{turb}})} \cdot \overline{DELQ}\right\}_{AMIP} \cdot \Delta\overline{|\vec{V}|} \\ & + L_v \cdot \left\{\bar{\rho} \cdot \overline{|\vec{V}|} \cdot \overline{DELQ}\right\}_{AMIP} \cdot \Delta\overline{C_{DE}(T_{s_{turb}})} \\ & + L_v \cdot \left\{\bar{\rho} \cdot \overline{|\vec{V}|} \cdot \overline{C_{DE}(T_{s\_turb})}\right\}_{AMIP} \cdot \Delta\overline{DELQ} + residual \quad (8)\end{aligned}$$

The changes in latent heat flux, $\Delta\overline{LE}$, are now decomposed into contribution from the changes in surface air density (the 1st term on the right hand side of (8)), surface wind speed (the 2nd term), bulk coefficient (the 3rd term), vertical contrast of specific humidity (the 4th term), and the residual. Each term in the equation (8) is calculated using the daily output from MIROC6, and the results are plotted in Figure S9. The figure shows that the decrease in latent heat flux, $\Delta\overline{LE}$, is mostly explained by the contribution from the changes in bulk coefficient (Figure S9ad). This result is consistent with the understanding that the longwave-induced warming of the atmosphere increases the static stability at the air-sea interface, which suppresses the turbulent transport of water vapor from the sea surface.

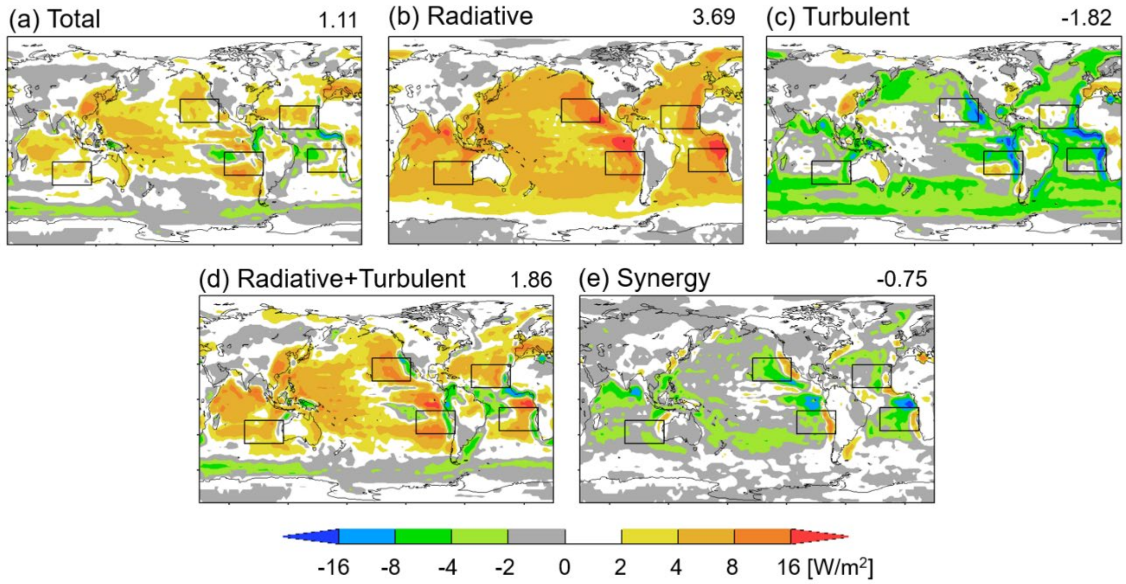

Figure S1. As in Figure 2, but the simulation data are created using MIROC5. Pattern correlation between (a) and (d) is 0.78.

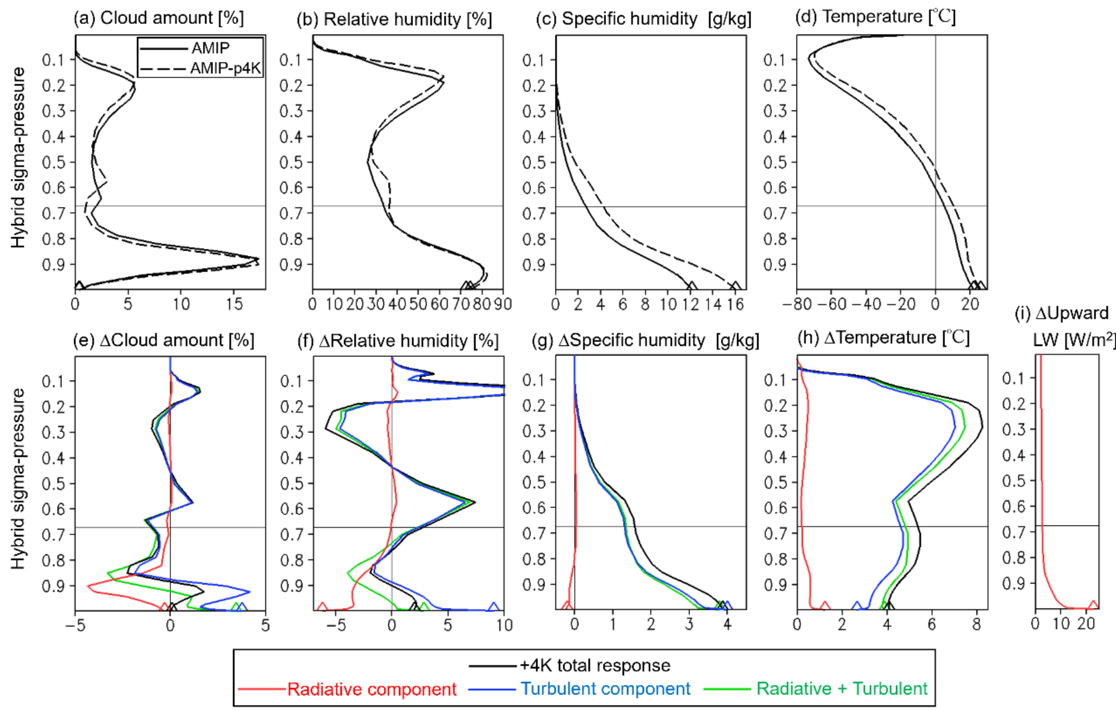

Figure S2. As in Figure 3, but the simulation data are created using MIROC5.

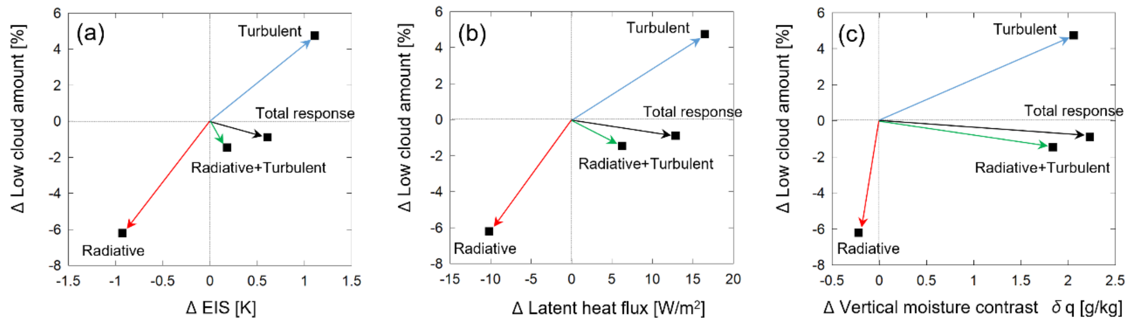

Figure S3. As in Figure 4, but the simulation data are created using MIROC5.

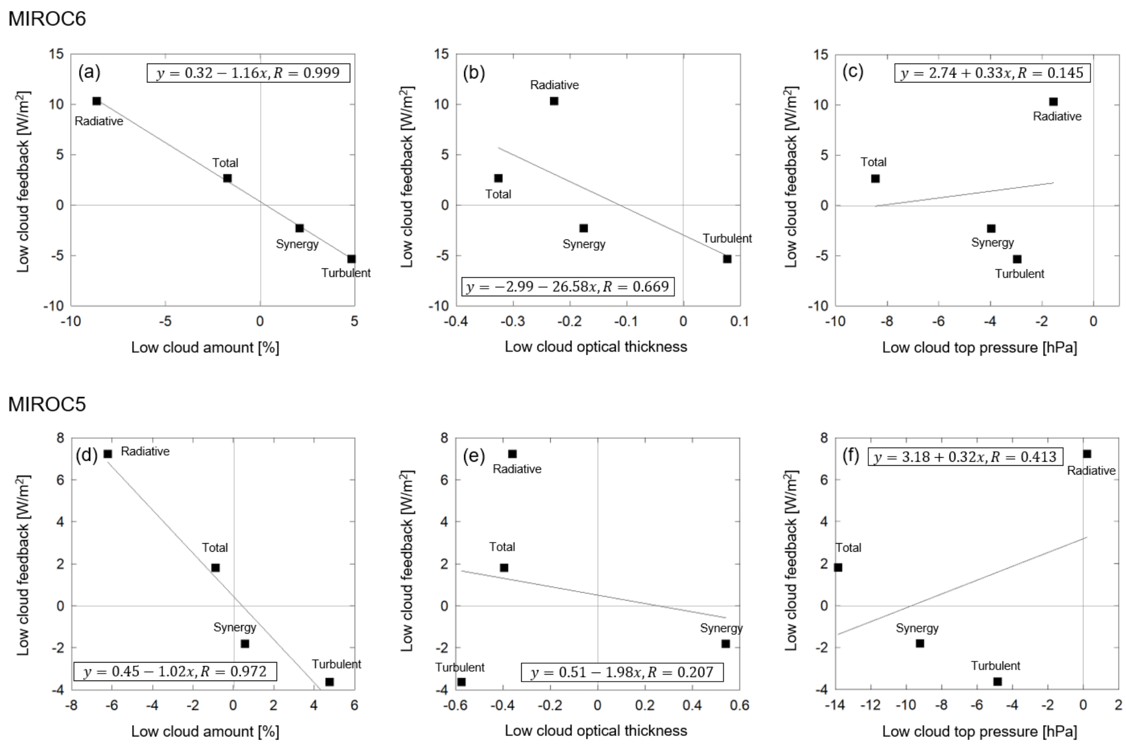

Figure S4. Relation between low cloud feedback and changes in (a)(d) low cloud amount, (b)(e) low cloud optical thickness, and (c)(f) low cloud top pressure, induced by SST+4K. The results are averages over the low cloud regions indicated by the black rectangles in Figure 2. The simulation data are created using (a)(b)(c) MIROC6 and (d)(e)(f) MIROC5. Regression equation and correlation coefficient are also shown in each panel.

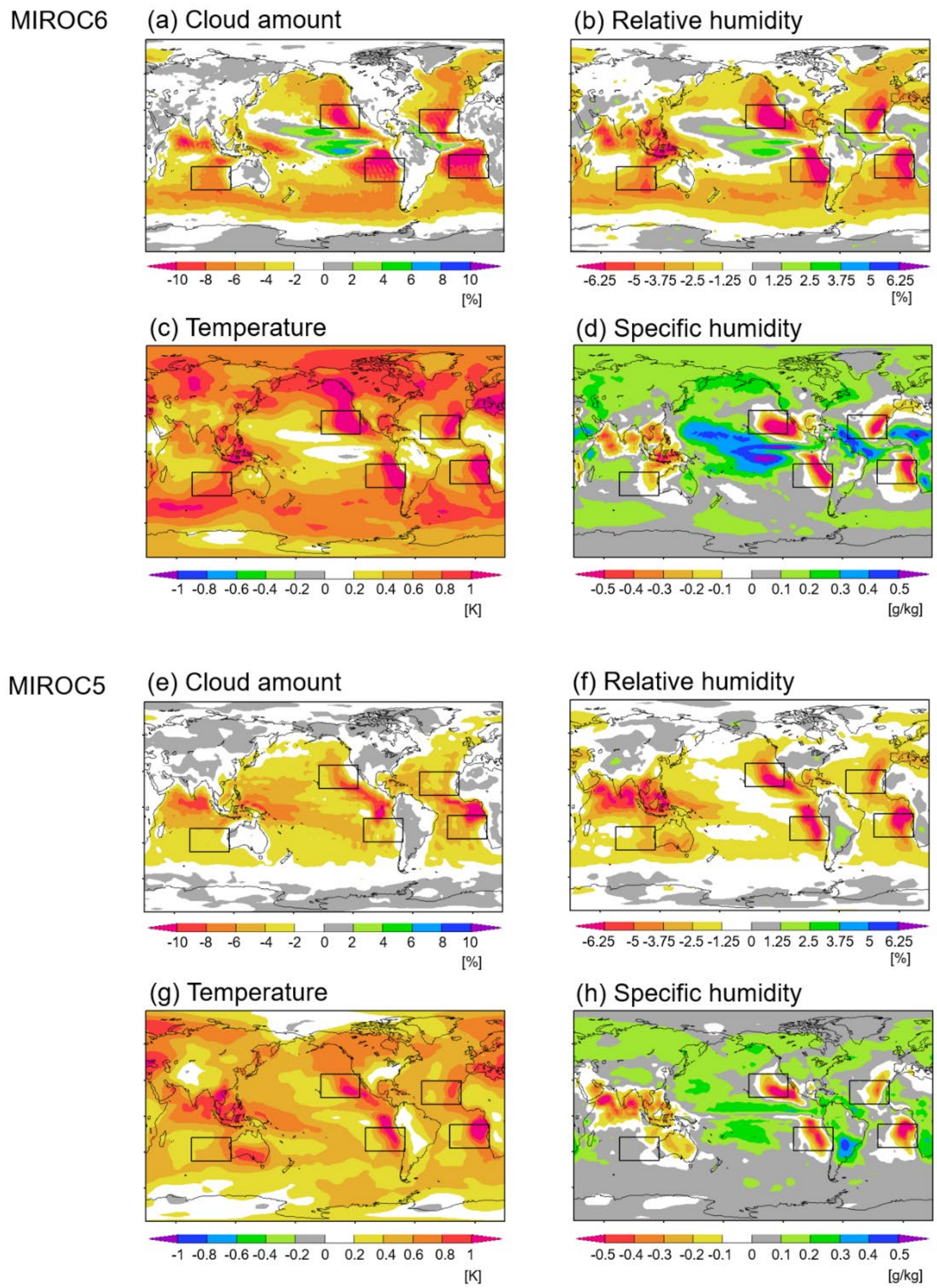

Figure S5. Radiative component of changes in (a)(e) cloud amount, (b)(f) relative humidity, (c)(g) temperature, and (d)(h) specific humidity, at the vertical σ-p level of 0.90. The simulation data are created using (a)(b)(c)(d) MIROC6 and (e)(f)(g)(h) MIROC5. Black rectangles indicate low cloud regions focused on in Figures 3 and 4.

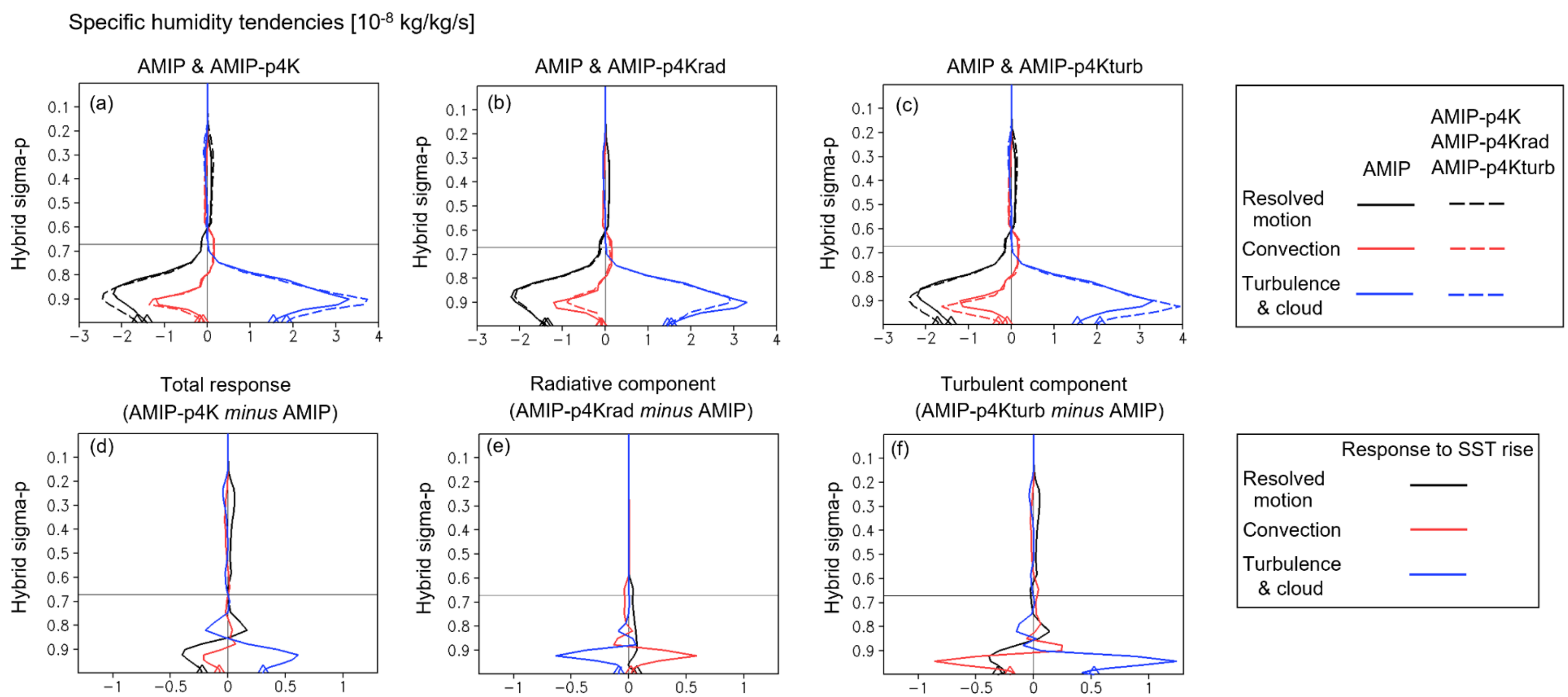

Figure S6. Specific humidity tendencies in (a) AMIP and AMIP-p4K, (b) AMIP and AMIP-p4Krad, and (c) AMIP and AMIP-p4Kturb experiments. Responses to SST +4K warming are also shown for (d) total response, (e) radiative component, and (f) turbulent component. The results are averages over the low cloud regions indicated by the black rectangles in Figure 2. The simulation data are created using MIROC6. Diamonds indicate values at the lowest level.

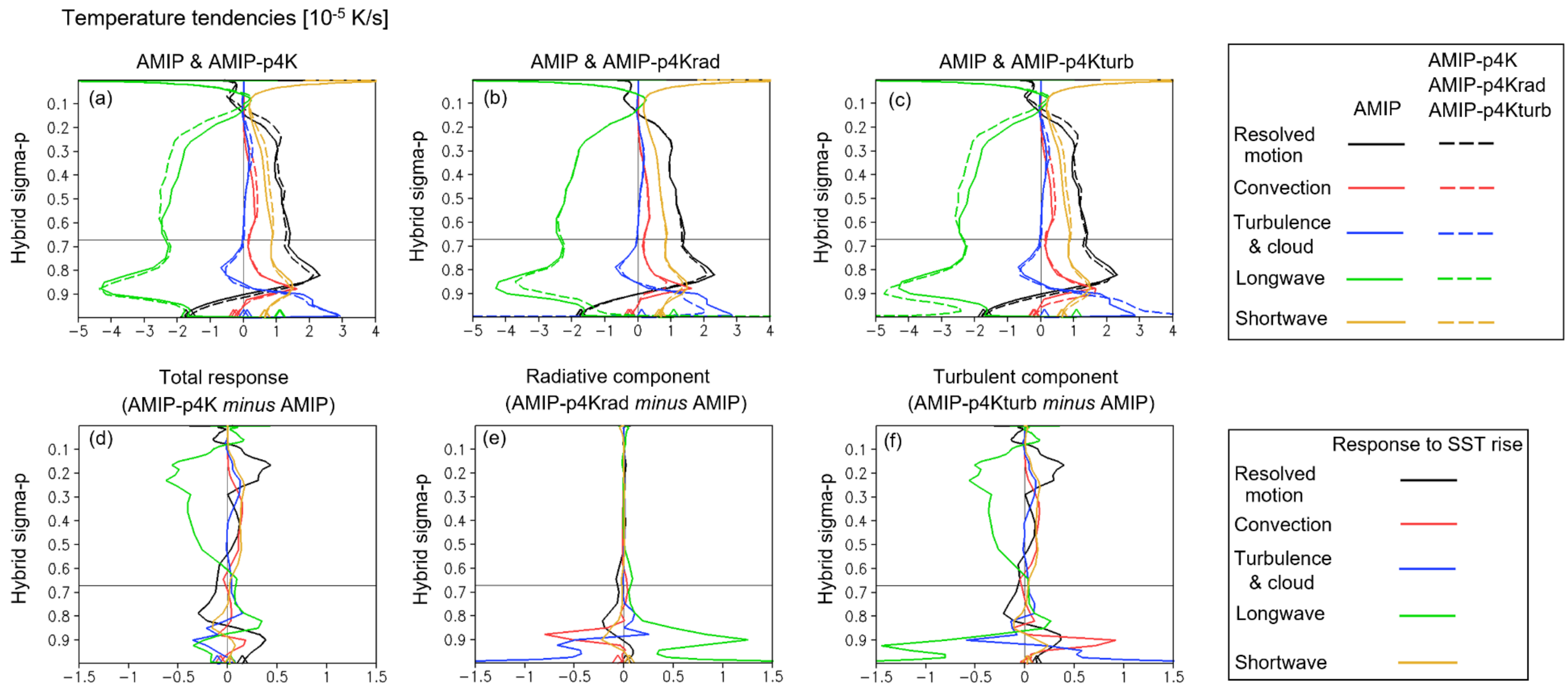

Figure S7. Temperature tendencies in (a) AMIP and AMIP-p4K, (b) AMIP and AMIP-p4Krad, and (c) AMIP and AMIP-p4Kturb experiments. Responses to SST +4K warming are also shown for (d) total response, (e) radiative component, and (f) turbulent component. The results are averages over the low cloud regions indicated by the black rectangles in Figure 2. The simulation data are created using MIROC6. Diamonds indicate values at the lowest level.

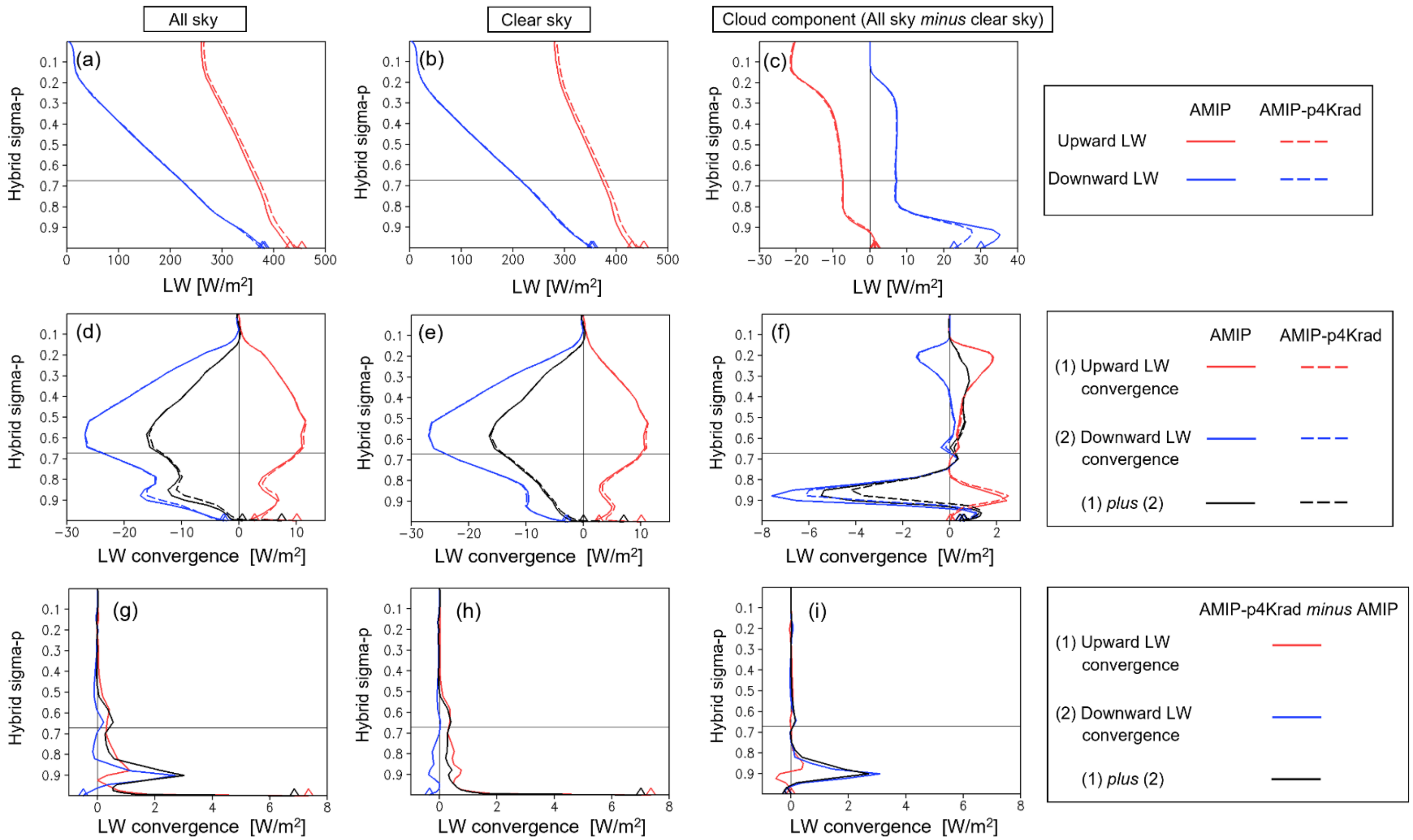

Figure S8. (a)(b)(c) Upward and downward longwave radiation, and (d)(e)(f) their vertical convergence in the AMIP and AMIP-p4Krad experiments. (g)(h)(i) Changes in the vertical convergence due to the SST warming in the AMIP-p4Krad experiment. Results are shown for (a)(d)(g) all sky, (b)(e)(h) clear sky, and (c)(f)(i) cloud component (all sky minus clear sky), averaged over the low cloud regions indicated by the black rectangles in Figure 2. The simulation data are created using MIROC6. Diamonds indicate values at the lowest level.

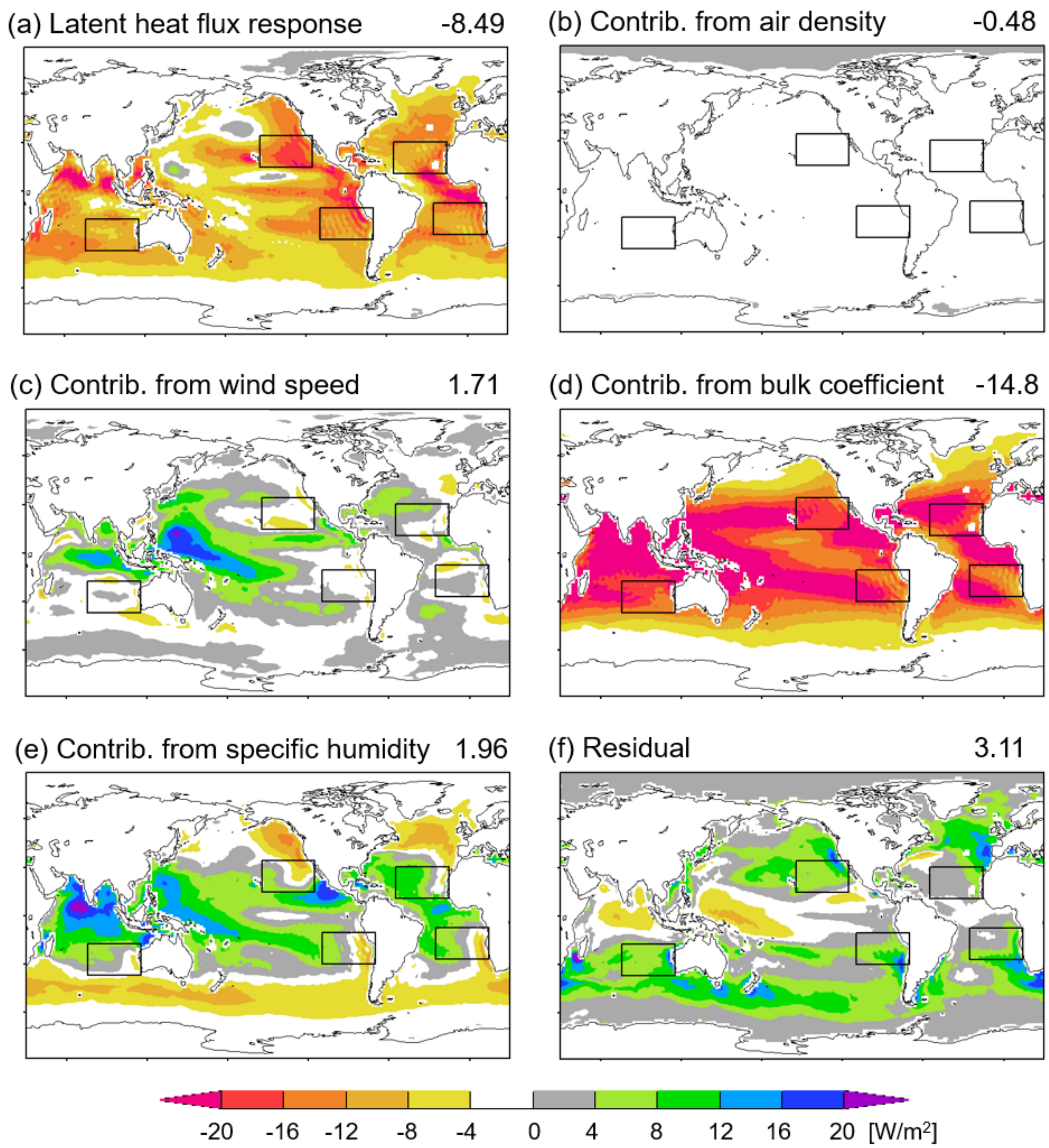

Figure S9. Changes in latent heat flux at the sea surface induced by SST warming of 4K. Results are shown for the radiative component, namely, AMIP-p4Krad minus AMIP. (a) changes in latent heat flux, (b) contribution to (a) from changes in surface air density, (c) contribution to (a) from changes in surface wind speed, (d) contribution to (a) from changes in bulk coefficient, (e) contribution to (a) from changes in vertical contrast of specific humidity, and (f) residual. Global averages are indicated at the top right of each panel. The simulation data are created using MIROC6. Definition of the quantities shown in panels (b)-(f) is given in Text S2.

Table S1. Examples of low cloud feedback mechanisms and how they relate to the present study

Mechanism	Is the mechanism consistent with the results of the present study? Namely, can the mechanism explain the low cloud changes in AMIP-p4Krad or AMIP-p4Kturb compared to AMIP?
Positive feedback due to low cloud decrease (Rieck et al. 2012) In the trade wind cumulus regions, if large-scale atmospheric processes act to keep relative humidity constant, atmospheric warming induces an increase in surface moisture fluxes. This drives a deeper boundary layer and hence mixes more dry and warm air from the free troposphere to the surface. As a result, shallow cumulus layers tend to have fewer clouds.	Yes and No. Consistent with the low cloud decrease in AMIP-p4Kturb(σ-p$\approx$0.85). Not consistent with the low cloud decrease in AMIP-p4Krad, because there is no increase in surface evaporation (Fig.S9a). Not consistent with the low cloud increase in AMIP-p4Kturb (σ-p$\gtrsim$0.9).
Positive feedback due to low cloud decrease (Webb and Lock 2013) Global mean surface evaporation increases with global temperature rise. However, in the subtropical stratocumulus/trade cumulus transition regions, the increase in evaporation may be less than the global mean because the Walker circulation weakens, which reduces both the near-surface wind speed and the air-sea temperature difference, while the near-surface relative humidity increases. As a result, the supply of water vapor from surface evaporation does not increase enough to maintain the low level cloud fraction in the warmer climate.	Yes and No. Consistent with the low cloud decrease in AMIP-p4Kturb(σ-p$\approx$0.85). Consistent with the low cloud decrease in AMIP-p4Krad, because reduction of the near-surface wind speed contributes to the decrease in surface evaporation (Figs.S9a,c). Not consistent with the low cloud increase in AMIP-p4Kturb (σ-p$\gtrsim$0.9).
Positive feedback due to low cloud decrease (Bretherton et al. 2013, Tan et al. 2017, Schneider et al. 2019)	Yes and No. Consistent with the low cloud decrease in AMIP-p4Kturb(σ-

Over marine boundary-layer stratocumulus cloud, the warmer free troposphere contains more water vapor, hence is more emissive. This increases the downwelling radiation from the free troposphere and reduces the net radiative cooling of the cloud-topped boundary layer, reducing the turbulence production. As a result, the entrainment rate decreases at the cloud top, leading to a lowering of the inversion and a thinning of the cloud layer.	$p \approx 0.85$). Not consistent with the low cloud decrease in AMIP-p4Krad, because there is little increase in water vapor specific humidity in the free troposphere (red curve in Fig.3g). Not consistent with the low cloud increase in AMIP-p4Kturb (σ-$p \gtrsim 0.9$).
Positive feedback due to low cloud decrease (Brient and Bony 2013) In a warmer climate, the non-linearity of the Clausius-Clapeyron relationship leads to a larger increase in specific humidity at high temperatures and low altitudes than at lower temperatures and higher altitudes. This leads to an enhanced vertical gradient of specific humidity and moist static energy (MSE) between the boundary layer and the lower free troposphere, and thus an enhanced import of low-MSE and dry air from the free troposphere down to the surface by large-scale subsidence. This decreases the low-level cloud fraction.	Yes and No. Consistent with the low cloud decrease in AMIP-p4Kturb(σ-$p \approx 0.85$). Not consistent with the low cloud decrease in AMIP-p4Krad, because there is no increase in vertical gradient of specific humidity (red curve in Fig.3g). Not consistent with the low cloud increase in AMIP-p4Kturb (σ-$p \gtrsim 0.9$).
Positive feedback due to low cloud decrease (Zhang et al. 2013, Brient et al. 2016, Vial et al. 2016). Higher SST causes a warmer climate, with a larger moisture contrast between the free troposphere and the boundary layer. The larger moisture contrast enhances the upward moisture flux by shallow convection or cloud-top entrainment at the level immediately above the top of the	Yes and No. Consistent with the low cloud decrease in AMIP-p4Kturb(σ-$p \approx 0.85$). Not consistent with the low cloud decrease in AMIP-p4Krad, because there is no increase in vertical moisture contrast (red curve in Fig.3g).

boundary layer. This causes larger ventilation of the cloud layer, which tends to decrease low cloud. The decrease in low cloud is accompanied by a reduction of radiative cooling by the low cloud. As a result, lower troposphere becomes stabilized. This weakens the latent heat flux from the sea surface, reducing the low cloud further.	Not consistent with the low cloud increase in AMIP-p4Kturb (σ-p$\gtrsim$0.9).
Positive feedback due to low cloud decrease (Vogel et al. 2019) In the downstream trade cumulus regions, sea surface warming leads to an increase in the surface fluxes, which deepens the shallow convection and increases precipitation. The increase in precipitation leads to a reduction of the detrained stratiform layers. In addition, the deeper clouds penetrate the inversion and detrain the moisture in the free troposphere, which further reduces the stratiform cloudiness.	No. Not consistent with AMIP-p4Krad or AMIP-p4Kturb, because low clouds do not deepen in either of the experiments compared to AMIP.
Negative feedback due to low cloud increase (Miller 1997, Klein and Hartmann 1993, Wood and Bretherton 2006, Qu et al. 2015, Tan et al. 2016) In low latitudes, the free-tropospheric temperature profile stabilizes with global warming. This increases the strength of the inversion capping the planetary boundary layer. As a result, vertical mixing across the inversion reduces, keeping the boundary layer shallower and more humid, which increases the stratiform low cloud cover.	Yes and No. Consistent with the low cloud decrease in AMIP-p4Krad, because the strength of the inversion decreases with warming (red curve in Fig3h). Consistent with the low cloud increase in AMIP-p4Kturb (σ-p$\gtrsim$0.9), because the strength of the inversion increases with warming (blue curve in Fig3h). Not consistent with the low cloud decrease in AMIP-p4Kturb(σ-p$\approx$0.85).
Negative feedback due to low cloud increase (Wyant et al. 2009,	Yes and No.

Narenpitak and Bretherton 2019). Higher SST causes a warmer and moister trade-cumulus boundary layer which experiences stronger net radiative cooling. The stronger cooling destabilizes the cumulus layer, leading to more vigorous convection. This fosters a moister boundary layer with more cumulus clouds, which amplifies the anomalous radiative cooling.	 Consistent with the low cloud increase in AMIP-p4Kturb (σ-p≳0.9). Not consistent with the low cloud decrease in both AMIP-p4Krad and AMIP-p4Kturb (σ-p≈0.85).
Negative feedback due to low cloud increase (Myers and Norris 2013) In the tropics, the atmospheric overturning circulation weakens as the climate warms. This leads to less subsidence over the subtropical marine boundary layer clouds, which allows a deeper inversion with more vertical development of the clouds, thickening the cloud layer.	No. Not consistent with AMIP-p4Krad or AMIP-p4Kturb, because low clouds do not deepen in either of the experiments compared to AMIP.
Negative feedback due to low cloud increase (Zhang et al. 2013). Higher SST causes a warmer climate. Accompanied by the weaker large-scale subsidence, the warmer climate has greater surface latent heat flux, larger turbulence moisture convergence in the cloud layer, and consequently an increase in low cloud.	Yes and No. Consistent with the low cloud increase in AMIP-p4Kturb (σ-p≳0.9). Not consistent with the low cloud decrease in both AMIP-p4Krad and AMIP-p4Kturb (σ-p≈0.85).

References

Bretherton, C. S., P. N. Blossey, and C. R. Jones (2013), Mechanisms of marine low cloud sensitivity to idealized climate perturbations: A single-LES exploration extending the CGILS cases, J. Adv. Model. Earth Syst., 5, 316-337, doi:10.1002/jame.20019.

Brient, F. and S. Bony (2013), Interpretation of the positive low-cloud feedback predicted by a climate model under global warming, Clim. Dyn., 40, 2415-2431, doi:10.1007/s00382-011-1279-7.

Brient, F., T. Schneider, Z. Tan, S. Bony, X. Qu, and A. Hall (2016), Shallowness of tropical low clouds as a predictor of climate models' response to warming, Clim. Dyn., 47, 433-449, doi:10.1007/s00382-015-2846-0.

Klein, S. A. and D. L. Hartmann (1993), The seasonal cycle of low stratiform clouds, J. Clim., 6, 1587-1606.

Miller, R. L. (1997), Tropical thermostats and low cloud cover, J. Clim., 10, 409-440.

Myers, T. A. and J. R. Norris (2013), Observational evidence that enhanced subsidence reduces subtropical marine boundary layer cloudiness, J. Clim., 26, 7507-7524, doi:10.1175/JCLI-D-12-00736.1.

Narenpitak, P., and C. S. Bretherton (2019), Understanding negative subtropical shallow cumulus cloud feedbacks in a near-global aquaplanet model using limited area cloud-resolving simulations, J. Adv. Model. Earth Syst., 11, 1600-1626, doi:10.1029/2018MS001572.

Qu, X., A. Hall, S. A. Klein, and P. M. Caldwell (2015), The strength of the tropical inversion and its response to climate change in 18 CMIP5 models, Clim. Dyn., 45, 375-396, doi:10.1007/s00382-014-2441-9.

Rieck, M., L. Nuijens, and B. Stevens (2012), Marine boundary layer cloud feedbacks in a constant relative humidity atmosphere, J. Atmos. Sci., 69, 2538-2550, doi:10.1175/JAS-D-11-0203.1.

Schneider, T., C. M. Kaul, and K. G. Pressel (2019), Possible climate transitions from breakup of stratocumulus decks under greenhouse warming, Nat. Geosci., 12, 163-167, doi:10.1038/s41561-019-0310-1.

Tan, Z., T. Schneider, J. Teixeira, and K. G. Pressel (2016), Large-eddy simulation of subtropical cloud-topped boundary layers: 1. A forcing framework with closed surface energy balance, J. Adv. Model. Earth Syst., 8, 1565-1585, doi:10.1002/2016MS000655.

Tan, Z., T. Schneider, J. Teixeira, and K. G. Pressel (2017), Large-eddy simulation of subtropical cloud-topped boundary layers: 2. Cloud response to climate change, J. Adv. Model. Earth Syst., 9, 19-38, doi:10.1002/2016MS000804.

Vial, J., S. Bony, J.-L. Dufresne, and R. Roehrig (2016), Coupling between lower-tropospheric convective mixing and low-level clouds: Physical mechanisms and dependence on convection scheme, J. Adv. Model. Earth Syst., 8, 1892-1911, doi:10.1002/2016MS000740.

Vogel, R., L. Nuijens, and B. Stevens (2019), Influence of deepening and mesoscale organization of shallow convection on stratiform cloudiness in the downstream trades, Q. J. R. Meteorol. Soc., 146, 174-185, doi:10.1002/qj.3664.

Webb, M. J. and A. P. Lock (2013), Coupling between subtropical cloud feedback and the local hydrological cycle in a climate model, Clim. Dyn., 41, 1923-1939, doi:10.1007/s00382-012-1608-5.

Wood, R. and C. S. Bretherton (2006), On the relationship between stratiform low cloud cover and lower-tropospheric stability, J. Clim., 19, 6425-6432, doi:10.1175/JCLI3988.1.

Wyant, M. C., C. S. Bretherton, and P. N. Blossey (2009), Subtropical low cloud response to a warmer climate in a superparameterized climate model. Part 1: Regime sorting and physical mechanisms, J. Adv. Model. Earth Syst., 1, 7, doi:10.3894/JAMES.2009.1.7.

Zhang, M., C. S. Bretherton, P. N. Blossey, P. H. Austin, J. T. Bacmeister, S. Bony, F. Brient, S. K. Cheedela, A. Cheng, A. D. Del Genio, S. R. De Roode, S. Endo, C. N. Franklin, J.-C. Golaz, C. Hannay, T. Heus, F. A. Isotta, J.-L. Dufresne, I.-S. Kang, H. Kawai, M. Köehler, V. E. Larson, Y. Liu, A. P. Lock, U. Lohmann, M. F. Khairoutdinov, A. M. Molod, R. A. J. Neggers, P. Rasch, I. Sandu, R. Senkbeil, A. P. Siebesma, C. Siegenthaler-Le Drian, B. Stevens, M. J. Suarez, K.-M. Xu, K. von Salzen, M. J. Webb, A. Wolf, and M. Zhao (2013), CGILS: Results from the first phase of an international project to understand the physical mechanisms of low cloud feedbacks in single column models, J. Adv. Model. Earth Syst., 5, 1-17, doi:10.1002/2013MS000246.